Part IV

Experimental Validation of the Theoretical Prediction with the Particle Image Velocimetry Technique

Chapter 9

Particle Image Velocimetry for Free Surface Flow of Avalanches

9.1 Introduction

Following the numerical simulations presented in the last Chapter, we continue the validation of the theory by means of different laboratory avalanche experiments. In this chapter we will particularly focus on the theory of *velocity measurements* during the motion of an avalanche. The velocity and depth are crucial to describe the dynamics and to draw conclusions about the flow behaviour of an avalanche. Our primary task in this and the following chapter is the measurement of these quantities and their comparison against the theoretical predictions. We are mainly interested to measure velocity distributions for unsteady and free-surface flows of avalanches.

The experimental method which will be described and applied here is the so-called *Particle Image Velocimetry* (PIV) technique with which the velocity field of the surface in a granular avalanche can be measured. This is an *optical* measuring system. The basic idea of this system is as follows: A part or the whole of the surface of a flowing granular avalanche is illuminated twice, at time t and time $t + \Delta t$. Then the two pictures (called "frame A" and "frame B") are captured by a camera. "Displacements" of identifiable points of the moving avalanche are calculated by comparing frame A and frame B via pattern recognition. The velocity of such a point is simply its displacement divided by the time difference Δt between both frames*.

It has already been mentioned in the preceding chapters, that the extended Savage-Hutter-theory is a continuum theory that models the granular avalanche as a deforming and flowing mass. The material is of MOHR-COULOMB type (i.e., simple plastic behaviour) with a dry COULOMB sliding law at the base. Furthermore, the conducted depth integration of the three-dimensional equations implicitly assumes a nearly uniform velocity profile through the depth of the avalanche. There are only two *phenomenological parameters* with which the *material response* of such a granular avalanche is described. If a spatially two-dimensional problem (i.e., a free-surface flow) is considered, then three equations remain (one for the height and two for the downslope and cross-slope components of the velocity) from which the complete flow behaviour of the avalanche at every instant of

*Note that some parts of this chapter also closely follow [21].

time may be determined, if appropriate boundary and initial conditions and the material parameters are given.

We intend to implement the PIV system to measure the dynamical quantities like velocity distribution and geometry of an unsteady and free-surface flow of granular avalanches over curved surfaces. In the sequel we consider the flow on an inclined plane that merges continuously into the horizontal run-out zone without lateral confinement, (i.e., completely free-surface flow) with deposition zone. To measure the velocity of such an avalanche which will be released from a hemi-spherical cap and flows down an inclined surface, a (2D-) PIV-system is used. Particularly, we are interested in the magnitude of the *surface velocity* of the avalanche. Furthermore, we intend to obtain information about the velocity profile through the depth by simultaneous measurements of the velocity from the surface and the base of the chute. The assumption of a uniform velocity profile through the depth influences the factor in front of the nonlinear terms in the equations of motion. In addition, the knowledge about this depth profile provides general information of the physics of granular materials. It may for example help us to answer the question, under which flow conditions the granular material behaves more fluid-like or more solid-like and how these conditions can best be mathematically described [21]. Another important point is the behaviour at the onset of the avalanche motion and in the deposition zone, where the avalanche comes to rest. The former flow situation may provide information about the initial conditions which are particularly important for numerical simulations, whereas the latter one is of practical importance for determining the run-out distance for the practitioners.

9.2 Review of the Particle Image Velocimetry Technique

At first, we briefly review some basic theoretical aspects of the PIV system. Some details are also taken from [21, 108] and TSI's manual for PIV [147]. The PIV system is an optical system that essentially interprets differences in light intensities as a pattern. The use of a transparent fluid is the common case in PIV. To generate a pattern in the transparent fluid, small non-transparent *tracer particles* are seeded in the fluid. The PIV theory is based primarily on two exceptionally important functions. Firstly, the *image intensity field* and, secondly, the *cross-correlation function*. The function describing the pattern mathematically is the image intensity field. Particular spots of brightness are interpreted as grey-scale patterns which, in general, move. Such a moving pattern can most easily be detected by comparing two consecutive frames captured by a camera. Then, the second task of the system is to decide which is the "correct" displacement (and hence velocity) among a certain set of possible displacements. This can mathematically be accomplished by constructing the cross-correlation function between two consecutive brightness distributions. To this end it is necessary to detect both a pattern on frame A and frame B and a difference between the patterns from both frames.

The *geometric imaging* scheme is sketched in Fig. 9.1. The whole region of interest (here the lightsheet) in the three-dimensional physical space with coordinates $\mathbf{X}, \mathbf{Y}, \mathbf{Z}$ is subdivided into smaller regions, the so-called "interrogation volumes". Such a volume is mapped with the imaging lens into the "interrogation area" in the two-dimensional image

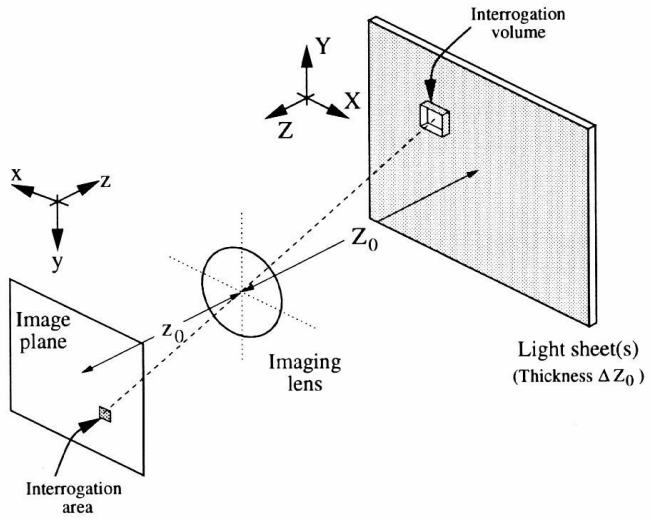

Figure 9.1: Sketch of the geometric imaging arrangement (from [108])

plane with the coordinates $\mathbf{x}, \mathbf{y}, \mathbf{z}$. For ease, in the following the phrase "interrogation spot" will be used for either interrogation volume or interrogation area.

9.2.1 Image Intensity Field

For each of the interrogation spots, the image intensity field assigns to each point in the image plane a scalar value which quantifies the light intensity of the corresponding point in the physical space. This light intensity depends on many factors, in particular the illumination, but also physical properties of the lens and the camera. However, for a series of experiments these latter influences can be kept constant. The image intensity field maps the light energy of an individual particle in the physical space (i.e., the tracer particles in the observed region of the flow) into an intensity value in the image plane. Mathematically, this function can be viewed as a transformation between two spaces. It is basically a convolution of the transfer function which is responsible for the determination of the "effective" light energy of one particle and the point spread function which describes the optical behaviour of the lens.

The image intensity fields $I(\mathbf{x}, \mathbf{\Gamma})$ and $I'(\mathbf{x}, \mathbf{\Gamma} + \mathbf{D})$ at times t and $t + \Delta t$ are defined, respectively, as follows:

$$I(\mathbf{x}, \mathbf{\Gamma}) = \sum_{i=1}^{N} V_0(\mathbf{X_i}) \tau(\mathbf{x} - \mathbf{x_i}) \tag{9.1}$$

$$I'(\mathbf{x}, \mathbf{\Gamma} + \mathbf{D}) = \sum_{j=1}^{N} V_0'(\mathbf{X_j} + \mathbf{D}) \tau(\mathbf{x} - \mathbf{x_j} - \mathbf{d}), \tag{9.2}$$

where $\mathbf{\Gamma} = (\mathbf{X_1}, \mathbf{X_2}, ..., \mathbf{X_N})$ denotes the position of the i^{th} (tracer) particle in the (three-dimensional) physical space, $\mathbf{x}$ the position in the (two-dimensional) image plane, $\mathbf{D}$ the

displacement in the physical space ($\mathbf{D} = \mathbf{X'_i} - \mathbf{X_i}$), $\mathbf{d}$ the displacement in the image plane, V_0 the transfer function and τ the point spread function of the lens.

In this way one finally obtains a field of numbers in the interrogation area for each pixel and each point of time. These numbers may be considered as grey values, and the whole set may be interpreted as a *grey scale pattern* [21]. It is in general moving and/or deforming (i.e., a function of time). However, it is common practice to assume that all points in this spot are assigned the same velocity, i.e., this pattern is moving "rigidly" in the interrogation spot.

9.2.2 Cross-Correlation Function

The cross-correlation function $R_{II}(\mathbf{s}, \mathbf{\Gamma}, \mathbf{D})$ is defined as the convolution

$$\begin{aligned} R_{II'}(\mathbf{s}, \mathbf{\Gamma}, \mathbf{D}) &= \frac{1}{\alpha_I} \int_{\alpha_I} I(\mathbf{x}, \mathbf{\Gamma})\, I'(\mathbf{x} + \mathbf{s}, \mathbf{\Gamma} + \mathbf{D})\, \mathrm{d}\mathbf{x} \\ &= \frac{1}{\alpha_I} \sum_{i,j} V_0(\mathbf{X_i})\, V_0'(\mathbf{X_j} + \mathbf{D}) \int_{\alpha_I} \tau(\mathbf{x} - \mathbf{x_i})\, \tau(\mathbf{x} - \mathbf{x_j} + \mathbf{s} - \mathbf{d})\, \mathrm{d}\mathbf{x}, \end{aligned} \quad (9.3)$$

where α_I denotes the interrogation area and $\mathbf{s}$ the separation vector in the correlation plane. The function $R_{II'}$ essentially calculates possible displacements by correlating all "grey values" from the first frame (intensity field I) with all "grey values" from the second frame (intensity field I'), where the separation vector is the independent variable that is to be varied. To make this clear, consider a simple example as is illustrated in Fig. 9.2. Suppose that three particles are located at $\mathbf{x_1}$, $\mathbf{x_2}$ and $\mathbf{x_3}$ in an interrogation spot at time t, i.e., picture I in Fig. 9.2a. At time $t + \Delta t$, they have moved to the positions $\mathbf{x'_1}$, $\mathbf{x'_2}$ and $\mathbf{x'_3}$ in Fig. 9.2a. In passing (i.e., picture I' in Fig. 9.2a) we note that $\mathbf{x'_2}$ is not inside the interrogation spot. This is called "loss of pairs". However, the cross-correlation function $R_{II'}$ shown in Fig. 9.2b is calculated by taking *all* possible displacements *regardless* whether the correct particles are correlated with each other or not, i.e., if the particle at

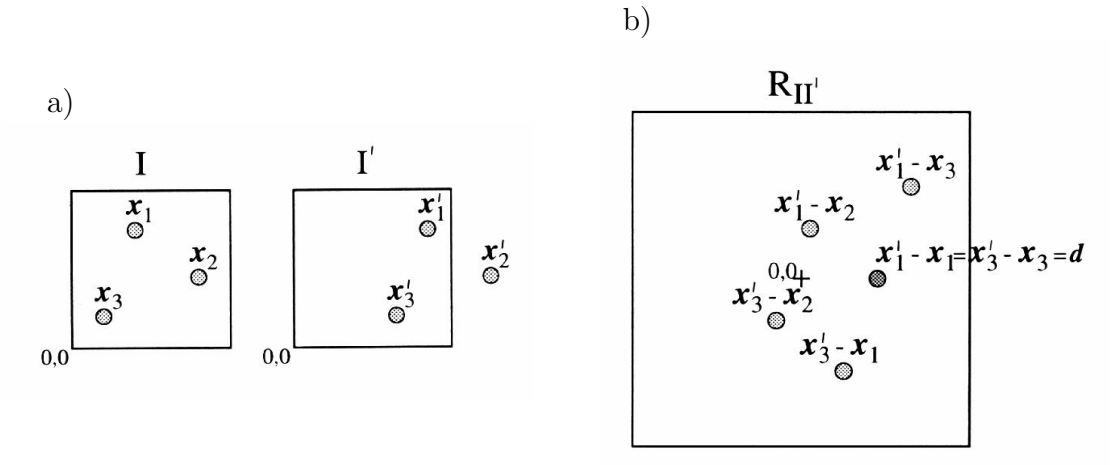

Figure 9.2: a) Image intensity fields I and I' at times t and $t' = t + \Delta t$, respectively. b) The corresponding cross-correlation of all possible displacements (from [108])

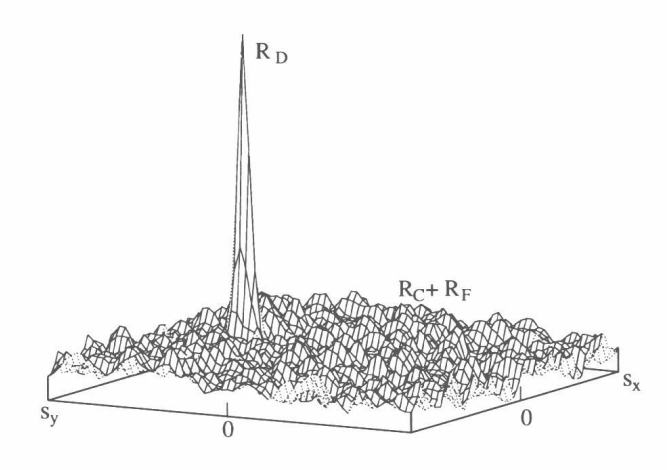

Figure 9.3: An example of the cross-correlation plane illustrating the correlation of identical particle images R_D and the errors $R_C + R_F$ (from [108])

$\mathbf{x_1}$ would have moved to $\mathbf{x'_3}$, then the displacement would be $\mathbf{x'_3} - \mathbf{x_1}$ and so on. Four of the six possible displacements occur only once, but $\mathbf{x'_1} - \mathbf{x_1} = \mathbf{x'_3} - \mathbf{x_3} = \mathbf{d}$ occurs twice. Thus, the displacement d is the most likely displacement.

$R_{II'}$ can be decomposed into three parts (see [63]):

$$R_{II}(\mathbf{s}, \mathbf{\Gamma}, \mathbf{D}) = R_D(\mathbf{s}, \mathbf{\Gamma}, \mathbf{D}) + (R_C(\mathbf{s}, \mathbf{\Gamma}, \mathbf{D}) + R_F(\mathbf{s}, \mathbf{\Gamma}, \mathbf{D})), \tag{9.4}$$

where R_D is the correlation of identical particle images (terms $i = j$), R_C the convolution of the mean intensities (terms $i \neq j$) and R_F the fluctuating noise (terms $i \neq j$). This means that $R_C + R_F$ produce the errors, whereas R_D is the correct value which is sought. Figure 9.3 shows a picture of the cross-correlation plane. R_D corresponds to the highest value of $R_{II'}$ in the correlation plane which is called "first peak". The coordinates s_x and s_y are the separations in the x- and the y-directions, respectively. This picture can be read as follows: The most likely displacement is the displacement $d = (s_x(R_D), s_y(R_D))$, where $s_{x,y}(R_D)$ denote the coordinates of R_D in the cross-correlation plane. The quality of this measurement is usually estimated by determining the ratio of the value of the first peak divided by the value of the second tallest peak (called first noise peak, tallest peak of the "noise" $R_C + R_F$): A high ratio means high and a low ratio means low reliability of the measurements.

9.2.3 Spatial Resolution

It is to be noted that *only one* displacement vector is calculated within one interrogation spot. The velocity vector is simply the displacement vector divided by the time delay Δt between two frames. It must hence be viewed as an average velocity vector of the particles inside the interrogation spot. To increase the *spatial accuracy*, especially for flows with strong displacement gradients, the interrogation spot size must be chosen sufficiently small. Common values are 32×32 and 64×64, for example. If the camera resolution is 1280×1024 and the observed region fits the whole image zone, then $40 \times 32 = 1280$ and $20 \times 16 = 320$ velocity vectors are calculated for interrogation spot sizes of 32×32 and 64×64, respectively [147].

9.2.4 Summary of the PIV System

The mathematical procedure of the PIV system can be summarised as follows [21]:

- Subdivide the whole area/image into interrogation spots.
- Calculate the image intensity fields at time t and $t + \Delta t$ for one interrogation spot.
- Calculate the correlation between these image intensity fields for one given separation.
- The cross-correlation plane is built by the correlation values of all possible separations.
- The most likely displacement is the separation for which the correlation function has the highest value.
- Repeat the procedure for each interrogation spot.

9.3 Experimental Setup for Granular Avalanches

The PIV-setup for granular avalanches flowing down inclined surfaces is described in this section. First the "usual" PIV setup for transparent fluids is introduced. Subsequently it will become clear that there are specific problems occurring for (usually) "non-transparent" granular materials. For the granular avalanche experiments we make use of the plexiglass chutes. Furthermore, there are some particular problems concerning the usage of plexiglass chutes, which will also be discussed in this section. However, plexiglass chutes are used because they can be easily deformed to make different channels and the velocity fields can be measured simultaneously from above and below the chute.

9.3.1 Transparent Fluids and Usual PIV Setup

First, we briefly review a usual setup in a tunnel. A sketch is given in Fig. 9.4. The major device of the PIV-system is the camera. Together with lenses this is called *imaging optics*. For illumination, a laser including light sheet optics and a mirror are needed. To control and trigger the laser and the camera, a synchroniser and a PC with evaluation and postprocessing software should be installed. The transparent fluid must be seeded with tracer particles so that the camera and the software can detect some pattern.

9.3.2 Setup for Granular Avalanches

Now, we describe the PIV-setup which we used for granular materials. The setup for granular materials differs from that described above in the following respects: For non-transparent materials, laser light sheets can obviously not be used for illumination. Therefore, we employed computer controllable flashes which were equipped with a diffuser. In order to guarantee nearly the same brightness on both frames, the intensity and the flash duration of the flashes could be adjusted. From Fig. 9.4 it is clear that for "usual PIV" the velocity distribution of the tracer particles inside the flow is measured. But for "Granular-PIV" it is not possible. Alternatively, we measure the velocity of granular

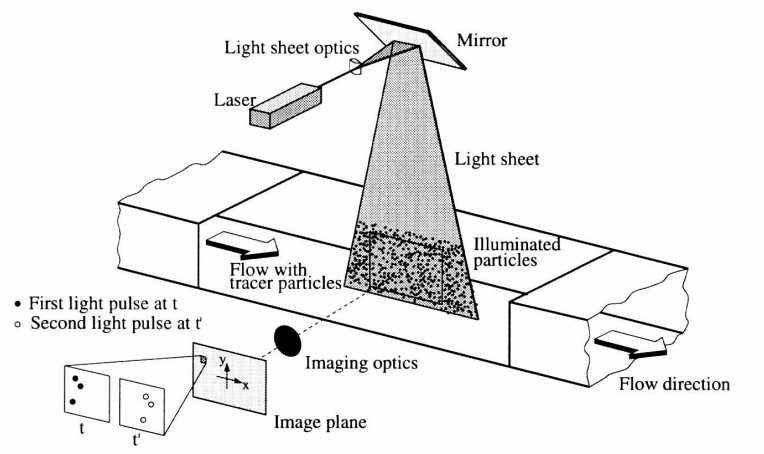

Figure 9.4: Usual PIV-setup in a wind tunnel with tracer particles (from [108])

particles of avalanching flow at the surface or at some boundary and the base, i.e., from below the plexiglass chute. It is advantageous with the granular particles that the optical surface structure that is produced by illumination of the surface of the avalanche is already sufficient to detect the motion. This means we do not need to add tracer particles in the bulk material. However, the flash illumination in connection with the plexiglass chutes that were used may produce different kinds of illumination errors that will be discussed later in greater detail. Furthermore, the region outside the support of the avalanche in the chute can be disregarded in the evaluation and post processing stage so as to eliminate (or to minimise) such errors.

9.3.3 Technical Details

It is perhaps appropriate to describe the technical details about the electronic equipments that were employed in the experiments. We use a system of the company TSI (see [147]). It includes two Charge Coupled Devices (CCD-cameras) of type TSI PIVCAM 13-8, two NIKON wide-angle lenses NIKKOR AF 28mm f/2.8D (henceforth called WA-lenses), see [96], a synchroniser and a PC including the INSIGHT PIV-software. For illumination we used either 2 or 4 flashes (if using either 1 or 2 cameras) of the type METZ MECABLITZ 60 CT-4, see [95]. As already explained we need two flashes for one camera since a camera captures two frames. Because the time delay between frames A and B is rather short, one might think it is sufficient to use one flash for illuminating both pictures. For two reasons this is not possible. Firstly, it is nearly impossible to trigger and adjust one flash such that the brightness on both pictures would be the same. Secondly, the shutter of the second frame is open for a relatively long time due to technical reasons which would result in distortions if only one flash would be used. The motion can in general not be frozen in time and the second picture becomes blurred [21]. Hence, the proper adjustment of the flashes is mandatory. The system is also supplemented by super-wide-angle-zoom lenses of type NIKON NIKKOR AF 18-35 mm f/3.5 $\sim$ 4.5D IF (henceforth called WAZ-lenses), see also [96]. In fact, these lenses were used in all experiments because of their greater variability and quality compared with the WA-lenses. As explained in Subsection 9.2.3, the CCD camera (we used) has a resolution of 1280×1024 pixel and a colour depth of

12 bit ($2^{12} = 4096$ different grey values). Furthermore, its highest temporal solution is 4 double frames per second. The time delay between the first and the second frame depends on the range of the velocity values. We have chosen it to be in the order of 1 micro second.

9.4 Experimental Peculiarities Arising for Granular Materials

As in every other measuring system, PIV is subjected to certain measurement uncertainties which cause errors. Some of them are specific for granular avalanches and some are of general relevance. There are two main error sources for Granular-PIV: Inappropriate surface structure of the avalanche and/or the background and imperfect illumination due to shadows, reflections etc. (also, see [21]). Both are specific for granular avalanches. Because of their exceptional importance, they will be discussed in the sequel in more detail.

9.4.1 General Errors

Below we point out some error sources of general relevance arising both in the transparent and non-transparent fluids like granular avalanches:

- Motion perpendicular to the picture plane (2D measurements): This is only of importance for locations where strong gradients of the height arise, i.e., in the outlet and deposition zones. However, even in this situation the influence is rather small in comparison with the main error sources.
- Displacement gradients arising within the interrogation spot: The pattern is not only shifted, but also deforming: This error is of limited importance at fixed boundaries of the domain.
- Angle between the observation plane and the camera is not 90 degrees: This is a big error source when the chute is relatively large and the space available for the experimental set-up is small. This is also a big problem for curved, and curved and twisted chutes and channels. In this case many cameras are needed, each for a very small portion of the flow domain.
- Distortion due to the usage of extreme wide angle lenses and short distances between camera and observation plane: As in the previous case, this causes problems for large chutes and small available experimental space.

9.4.2 Particular Errors for Granular Flows

Error from Light Reflection

There are still many other problems for Granular-PIV, e.g., light reflections from the chute or from the laboratory environments. Reflections can in general be avoided by either choosing an appropriate position of the flashes or using indirect flashing which does not point directly to the chute, but is directed towards a white paper or screen which reflects the flash light to the chute. This well-known procedure diffuses the light such that the chutes are in general illuminated with no or very few reflections [21].

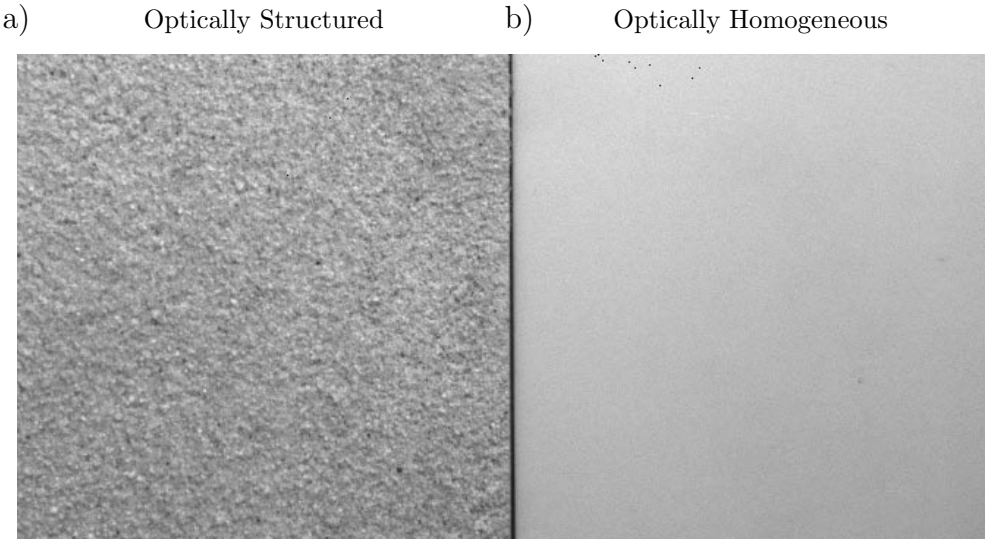

Figure 9.5: Two different surfaces at rest, coated with a) sand and b) varnish (from [21])

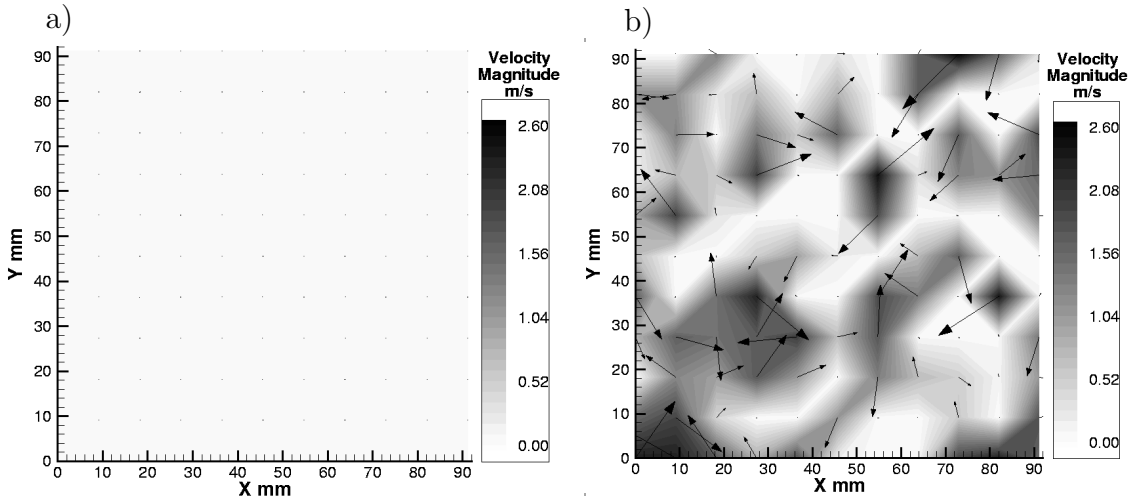

Figure 9.6: Measured velocity for, a) the sandpaper (corresponding to Fig. 9.5a) and, b) the varnish (corresponding to Fig. 9.5b) (from [21])

Error from Electrostatic Charging

Another specific problem, in case of fine materials flowing over plexiglass chutes is the electrostatic charging. This is more pronounced in case of two-dimensional channelised flow originated from a silo. Electrostatic charging can be minimised by using an anti-electrostatic charging spray.

Optical Surface Properties

The optical surface properties are of extraordinary importance. To illustrate this, velocity measurements of two plates which are at rest are compared [21]. One plate is covered with sand, the other one with a varnish. Whereas the surface of the former is optically quite structured, the surface of the latter is rather homogeneous, see Fig. 9.5.

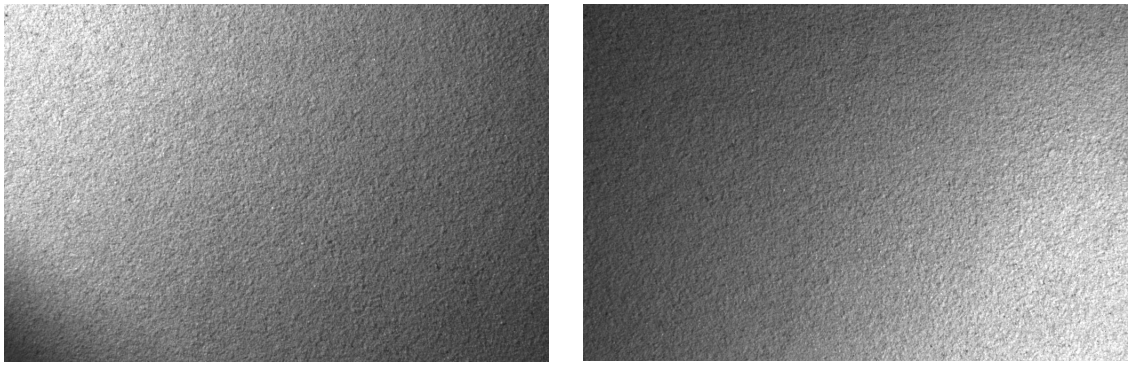

Frame A Frame B

Figure 9.7: Flash A upper left corner, flash B lower right corner of the observed region of a sandpaper surface at rest (from [21])

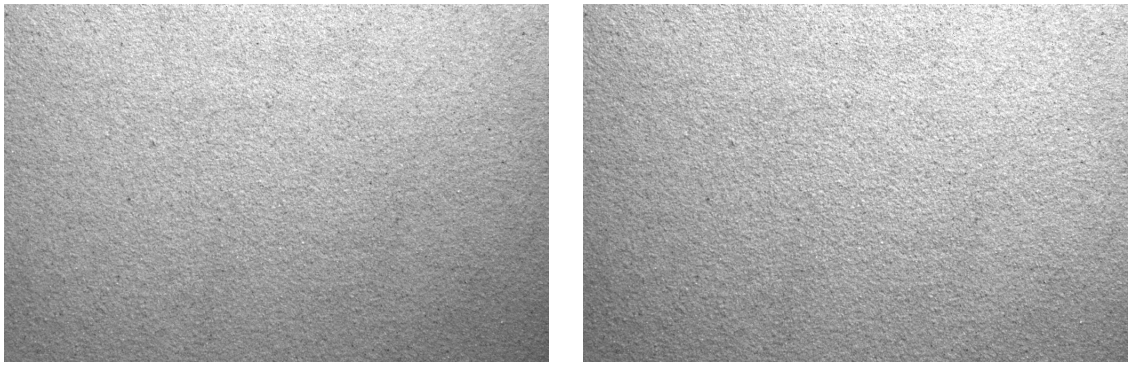

Frame A Frame B

Figure 9.8: Flashes as close as possible to each other, illuminating a sandpaper surface at rest in a possible homogenuous way (from [21])

The velocity distribution is given in Fig. 9.6. Whereas the velocity for the "sandplate" is measured correctly, the velocity of the varnished plate is not: the in-plane velocities are more or less randomly distributed in magnitude and orientation, which is clearly wrong. Even with an optically homogeneous (i.e., not-structured) background, still erroneous velocity vectors may be produced; this may deteriorate the whole quality of the measurements. It is thus recommended to choose also the background appropriately, i.e., with an optical structure if possible. However, this is not possible in case of plexiglass chutes. Nevertheless, in many situations we can either eliminate or minimise such errors by disregarding the grain-free zone of an avalanche in the post-processing operations.

Illumination

The other main error source is the illumination. If laser light sheets can be used, the quality of the illumination may in general be good. We are compelled to use alternative illumination techniques like flashes to illuminate the surface of non-transparent materials. Frame A and frame B of one double frame are shown for different positions of flash A and flash B on the two Figs. 9.7 and 9.8. The object illuminated is a sandpaper at rest. To

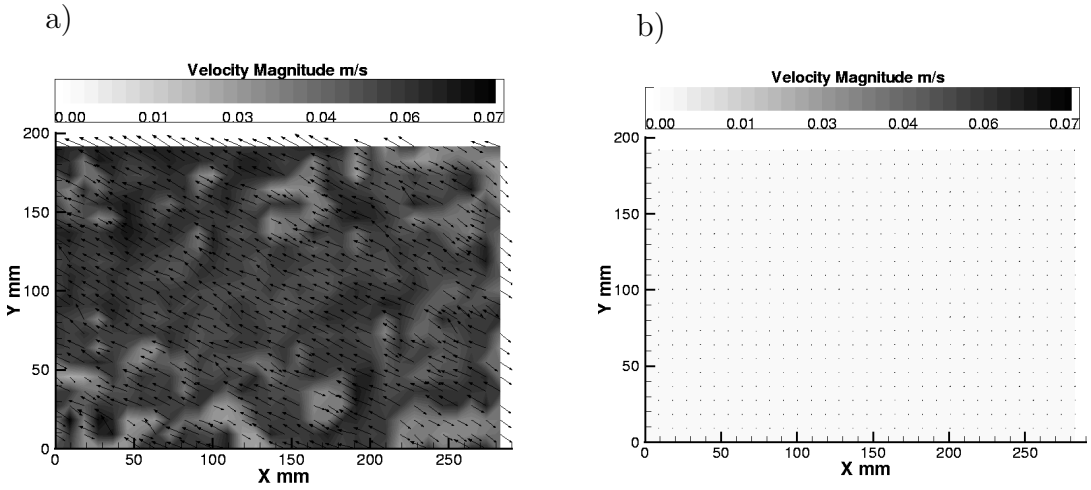

Figure 9.9: Measured velocity of sandpaper, a) for case of Fig. 9.7 and b) for case of Fig. 9.8 (from [21])

illustrate the effect in a drastic way, the position of the flashes are chosen "exaggeratedly bad". The illumination of subregions on the sandpaper is not the same for frame A and frame B in Fig. 9.7, whereas it is fairly uniform in Fig. 9.8. Note that illumination differences between different regions on the sandpaper are of minor importance; crucial is the comparison of the same subregion in frame A with that in frame B.

Figure 9.9 shows the measured velocity distribution of the sandpaper for the different positions of the flashes. It clearly shows, that inappropriate positions of the flashes lead to significant measurement errors. Notice that the error produced here is not of a random nature as was the case in the last paragraph. The direction of the "faulty velocity" distribution in Fig. 9.9a somehow reflects the axis and orientation of the flash illumination.

Testing the PIV-System

In this paragraph a simple method is described to estimate systematic errors of the measured velocity values of the PIV-system. Specifically, the deviation of velocity values of the surface from the bottom at the same spatial locations (which also may include the influence of the plexiglass) and the deviation of the velocity values from one another in the whole region of either the surface or the bottom is of interest for us. This will be dealt in greater detail in the next chapter while measuring the velocity distribution of a free-surface flow of avalanche over a curved plexiglass chute.

Towards this end, a setup with two cameras, a plexiglass chute and a "rigid avalanche" (see Fig. 9.10) is used. One camera is put below the chute (capturing pictures through the plexiglass) and the other one above it. If the sandpaper is released, double frames of both cameras are taken (simultaneously) from which the frames A are shown in Fig. 9.11. The measured velocity distribution is given in Fig. 9.12. Note that the range of the legends is from the lowest (1.833 ms^{-1}) to the highest value (1.898 ms^{-1}) measured value and that *raw data* were used, i.e., no filters have been applied to the data shown in Fig. 9.12. The deviation between the mean surface and the mean bottom velocity is only 0.13%. However, the deviation between the smallest and the highest velocity value

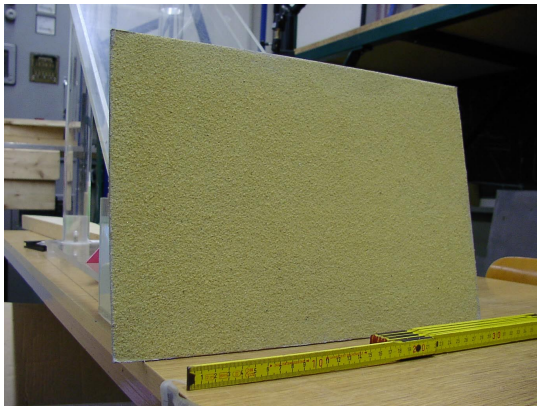

Figure 9.10: The "rigid avalanche": A thick piece of rigid paper (0.3 mm thickness) with sand both sides (from [21])

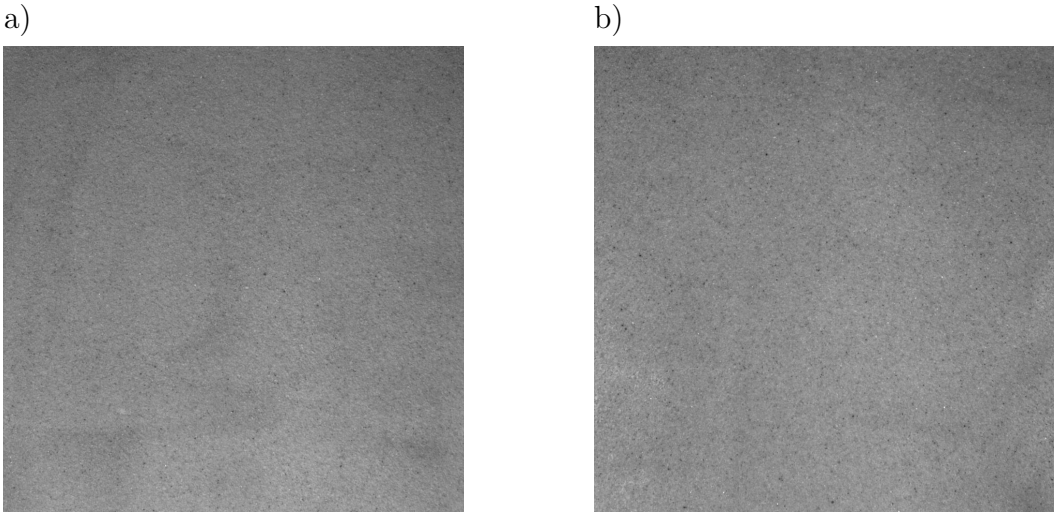

Figure 9.11: Frame A of a) the bottom and b) the surface camera (not mirrored). Motion is from top to bottom (from [21])

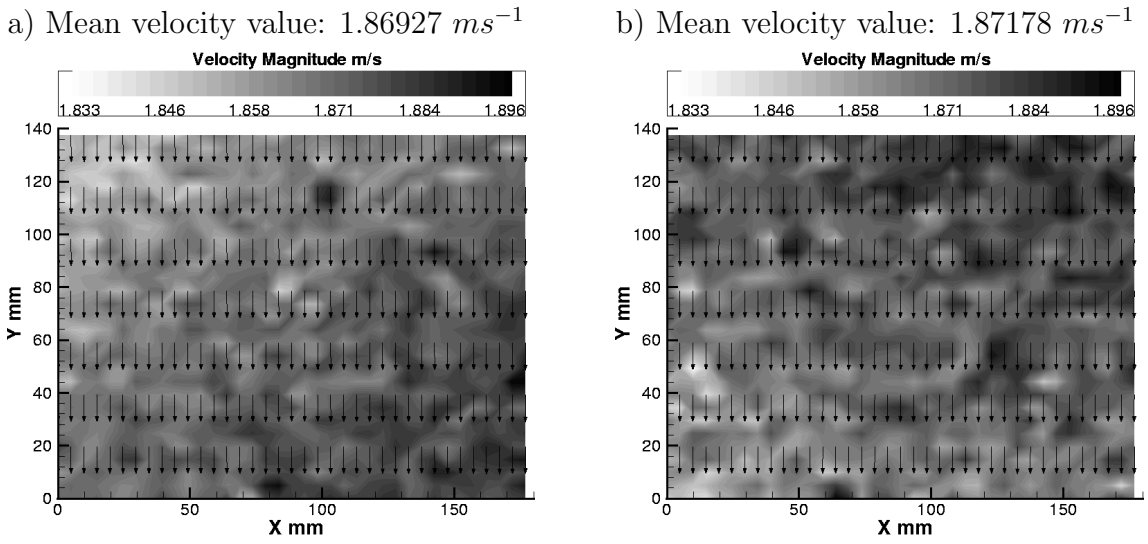

Figure 9.12: Measured velocity of a) the bottom and b) the surface of the sandpaper (not mirrored). Motion is from top to bottom (from [21])

in either panel a) or b) is approximately 3.5%. This shows once again that surface properties and the illumination which are responsible for the latter deviation are the main error sources, whereas the influence of the plexiglass is negligible.

9.5 Postprocessing and Evaluation

At the instant when the material is suddenly released (i.e., by lifting the cap), a sequence of a required number of pictures is captured. The most important data that can be obtained from Granular-PIV measurements is the surface velocity distribution. The camera produces 12-bit pictures. After capturing, the interesting portion of the pictures is subject to the calculation and validation processes to obtain the velocity (done by the software). A cross-correlation algorithm utilising *Fast* FOURIER *Transform* (FFT) is used [147]. The spot size of the interrogation windows is either 32×32 pixels (no oversampling) or 32×16 (double oversampling). After filtering possible errors, the processed files are exported to suitable plot programs for postprocessing operations.

In a PIV system, the raw data may be subjected to a so-called validation procedure to eliminate possible faulty data. This is done by filters. There are different filters, but two of them are important for us, namely the *range filter* and the *standard deviation filter*. With the range filter, the permissible range of velocity values can be adjusted. Sometimes selection of this range depends on one's own experience. It is to be mentioned that the avalanche is always flowing from top to bottom, say in the negative y-direction. This clearly suggests to restrict the velocity values in the y-direction to negative values. By definition, the standard deviation filter eliminates all velocity values that are not within a certain distance to the mean velocity. It can only be applied if the velocity values are not extremely differing from one another. In our case, the flow field is homogeneous, and thus the standard deviation filter provides a good choice to eliminate random errors. The blanks were interpolated by a mean neighbourhood filter.

However, in the next chapter we do not use these filters and thus need not to validate the data for the free surface flow of avalanche. The reason for this is that we will select a grain free region (outside the boundary) of the avalanche and delete it from processing so that there are (almost) no faulty data remaining. In the sequel we will use this technique in order not to use artificially interpolated data. This also increases the reliability of the measurements.

9.6 PIV with Multi-Cameras

Finally, we explain how PIV measurements are made with many cameras. Multi cameras are to be used mainly for three purposes: (i) one camera is put below and the other one above the chute to measure simultaneously at the same location the velocity of the base and the surface of the avalanche, respectively. These measurements serve as additional experimental result from which we may decide whether the velocity profile is uniform through depth or not. (ii) Two cameras can also be used to obtain the three-dimensional stereographic images and the velocity fields. (iii) In case of large, curved, and curved and twisted channels one must make use of series of cameras so as to have good measurements of several sub-divided flow regions. We will be mainly concerned with points (i) and (iii).

Chapter 10

Avalanche Experiments Using the PIV Measurement Technique

10.1 Introduction

In this chapter we will measure the efficiency of the extended avalanche theory [101] presented in Chapter 4. There are two ways to check the validity of a theory. On the one hand, one can apply the theory in real practice and measure the distance between the theory and the reality, e.g., in some large-scale (natural) geophysical flows like debris flows or avalanches. On the other hand, the performance of the theory can be judged by comparing well controlled laboratory experiments against the theoretical prediction of the model equations via their numerical solutions. There are many factors that directly or indirectly influence the correspondence between theory and experiments: (1) Laboratory circumstances, the experimental set-up and the measurement technique are concerned with the technical part of the correspondence. (2) Similarly, the numerical method is responsible to solve the model equations appropriately without loosing the underlying physics of these equations. (3) The theoretical model is always the heart in the description of any physical process. Because the model equations are generally constructed with ample physical insight together with some advanced mathematical computations, one normally thinks them to possess the capacity of reflecting the natural phenomenon with high efficiency. The physical-mathematical model constitutes the scientific ground to present the new ideas. It is true that construction of a model is already a tough task. But, the question is: Does the model really work? This means: can we really predict the real processes in nature or in the laboratory by these model equations? If yes, it is wonderful; if not, then, the theory is practically useless at least from an engineering and physical point of view. Under favourable circumstances the theory may then at best be applicable for physical processes other than those originally anticipated. In this chapter we will corroborate the physical adequacy of the model equations, efficiency of the numerical method and the harmony of them with the laboratory experiments performed under essentially well controllable circumstances together with an advanced measurement technique. Ultimately, we will demonstrate that for the prediction of the avalanche geometry and velocity through time the theory, numerics and the experimental results are in very good agreement.

As explained in the last chapter, we will make use of the Particle Image Velocimetry (measurement technique) to measure the dynamics of the velocity distribution of the avalanching flow down a curved chute. The other important variable in the model equations is the evolution of the avalanche geometry from initiation to the run-out zone until it comes to rest as a deposit. We will present the results on both the velocity and the height of the free-surface flow of avalanches via comparison of the experimental findings against the theoretical predictions. To our knowledge, such results have not been presented before (in such detail by making direct comparisons with the theoretical predictions) in the literature of the dynamics of debris flows and avalanches.

10.2 Experimental Details

10.2.1 The Chute Geometry and Arrangement

We performed several series of experiments over a chute as shown in Fig. 10.1*. The chute is made of plexiglass (3.5 mm thick). For safety reasons and to avoid any spreading of particles on the floor, the side and the front edges of the chute are vertically erected by walls of plexiglass of thickness 5 mm. The chute consists of three different parts connected together. The inclination angle of the upper inclined plane portion is 45°; it merges continuously into the horizontal run-out zone. In the upper right part of the chute, an electric clock is mounted with two arms: the long arm makes one complete revolution in one second, whereas one unit of the short arm stands for the duration of one second. In the middle-top of the inclined portion hemi-spherical caps of different capacities (i.e., sizes) can be mounted to hold the initial mass of the granular material. These caps can suddenly be lifted by pulling the rope connected to the cap in such a way that the flashes, the cameras and the PC are all synchronised and start operating together. The dimensions of the chute are as follows: (a) Upper inclined part: length 1560 mm, (b) Continuous transition zone: (curved) length 370 mm, (c) Horizontal run-out zone: length 2250 mm. The width of all three parts is 1600 mm.

Due to its largeness the chute is divided into three zones: (i) upper inclined-zone, (ii) middle continuous transition-zone and (iii) lower horizontal run-out-zone. Experimental images are taken separately in all three zones but under (essentially) identical experimental conditions and laboratory circumstances. Such a division of the whole flow domain into three zones also increases the quality and reliability of the measurements. It should also be noted that, if one includes the entire flow region (i.e., the whole chute) in a single capture, the image and the data will be highly distorted because the chute is very large in dimension and consists of the inclined, transition and horizontal segments.

10.2.2 The Caps

Two kinds of caps are used separately to hold the granular materials at the middle-top of the chute, see Fig. 10.1. The caps are called "Small-Cap" and "Big-Cap", respectively, depending on their capacity (volume). Both caps are upper parts of different hemi-spheres. The Small-Cap is the top part (above 30° latitude) of a hemi-sphere of radius 195 mm.

*This chute was built by the workshop personnel Hartmut Hoffmann, Heinrich Wiener and Christof Bonk of the Department of Mechanics, Darmstadt University of Technology.

Table 10.1: Details of the granular materials used in different experiments. For rice the mean diameter means the mean diameter of the major axis

	Quartz	Yellow-Sand	Rice	Caps
Mean-Diameter (mm)	5	Fine	7	−−
Mass (kg)	8.72	8.91	8.30	Small-Cap
Mass (kg)	29.30	−−	−−	Big-Cap
Internal Friction Angle (ϕ)	35°	30°	40°	−−
Bed Friction Angle (δ)	23°	21°	22°	−−

The radius of the base of the cap thus constructed is 170 mm. The Big-Cap is constructed analogously from a hemi-sphere of radius 300 mm. The radius of the base of this cap is 260 mm. Note that this cap is the upper part of the corresponding hemi-sphere above 30° latitude measured from the horizontal. The geometries of these caps are designed in this way so that initially the granules at the front do not go through a free fall motion and that the bulk remains (almost) continuous at the time of lifting the caps. The caps are made of plexiglass with the supporting frame made of steel. These caps can instantly be lifted by applying a relatively heavy load connected to them by a rope from the forehead of the cap to its opposite side (backside of the chute) without making any disturbance to the flow. This motion in the opening process is a rotation about a horizontal axis.

10.2.3 The Materials

A series of experiments was conducted for three different types of dry granular materials with small and big caps, separately. The experiments are repeated for all three zones of the chute under essentially the same conditions. The materials used for the experiments are: Quartz, Yellow-Sand and Rice (long ellipsoidal). Table 10.1 presents the detailed information and other relevant statistics of the materials. Out of several experiments, only selected results will be presented.

10.2.4 Control and Synchronisation

The lifting of the cap, opening of the camera shutter, blinking of the flashes, starting of the clock and the connection of these devices with the computer are all synchronised[†]. All these are controlled and operated simultaneously. Such controls and synchronisations are *crucial* in determining the *real-time* of different *snaps* and positions of the avalanching mass. The real time elapse determined in this way is then used to find out the correspondence between the experiment and the theoretical prediction.

[†]The electronic instrumentation for this was built by the electronic technician Mr. K. Polster of the laboratory of the Department of Mechanics, Darmstadt University of Technology.

10.2.5 Velocity Measurements

As explained in the last chapter, the velocity of the avalanching and deforming granular material is measured by the Particle Image Velocimetry measurement technique of the company TSI. The velocity field of the particles at the free-surface and the bottom of the avalanche are measured. This provides information about the adequacy of one assumption of the SH-theory which is dealing with depth-averaged equations.

10.2.6 Measurement of Avalanche Depth Profiles

The temporal and spatial variations of the velocity distribution and the depth geometry describe the dynamics of the avalanche. If their prediction by the theory is correct then there must be a good correspondence between the avalanche depth predicted by the theory with that measured from the experiment at any instant of time. In particular, we are interested to have knowledge of the depth profile of the deposit of the avalanche in the run-out zone. Its correct determination is very important in real applications. There are two reasons for that: (I) When knowing the actual run-out distance (area) and the height profile of the deposit one can easily divide avalanche-prone mountain terrains and valleys into three zones: the avalanche danger zone, the less dangerous zone and the danger-free zone, i.e., one can construct the hazard map of the specific site. (II) On the other hand, if there is good agreement between the theory and the experimental measurement of the height profile in the deposit then one can easily infer the reliability and efficiency of the theory over the entire avalanche path. In this way the theory can be used to predict the velocity distribution, depth profile, impact pressure, strain rate and other related quantities as an avalanche slides down a mountain side.

For these reasons, we have measured the depth profiles of the deposits of avalanches of different materials, but only selected results will be presented here. The depth profile of each avalanche deposit is measured very carefully with a penetrometer. The measurements are done in an (approximately) optimal way in order not to disturb the neighbourhood geometry of the deposit during the entire measurement. In regions of large gradients of the granular pile heights relatively more points are taken. For each experiment, the depth measurements are taken at (about) 200 points. The data are interpolated and the geometries thus obtained are compared with the computed geometries of the theoretical predictions. Note also that the determination of the avalanche margin at each time step is very easy and can be identified by the margin of the velocity field measured by the PIV-measurements.

10.2.7 Non-Dimensional Parameters and the Length Scales

The model equations contain two non-dimensional parameters, ε and λ. They are associated with the geometry of the avalanching material and the chute. Provided the geometry is similar, the model equations (4.85)-(4.87) predict the same avalanche flow irrespective of whether it is in a small-scale laboratory run or a geophysical avalanche in a large-scale mountain environment (if we do not use a pressure or velocity dependent bed friction angle). To achieve possibly greater generality and a real feeling for the physical variables both the experimental and the computed results are presented in dimensional variables. The appropriate physical variables for a particular application can

then be constructed by applying the (back) transformation of the scalings (4.21). To make a correspondence between the theory and the experiment we must define a non-dimensionalisation of the physical variables. We chose the same length scale in all x, y and z directions, so $L = H = 10$ cm and $\mathcal{R} = 10$ cm. These length scales correspond to the characteristic lengths, the initial heights of the respective granular piles kept in the caps, providing $\varepsilon = H/L = 1$ and $\lambda = L/\mathcal{R} = 1$. This preserves the aspect ratio of the physical avalanche and makes it easier to interpret the results.

10.2.8 Determination of the Avalanche Boundary

One of the fundamental problems in avalanche experiments is the determination of the avalanche boundary. If the mass is relatively large, the granular particles are relatively smooth, the chute surface is smooth, the opening of the shutter holding the pile in its initial position is very fast and it can be lifted approximately vertically (relative to the chute) and the other mechanisms are also appropriately used, then, the demarcation between the grain-free and the avalanche zone is easy. Under such circumstances the granular body can not spread unsystematically near its boundary and the mass distribution around and along the boundary is fairly continuous. Otherwise, dispersion of the grains along the boundary is inevitable. Consequently, it is very difficult to define the boundary. If the boundary can not be determined properly one can not make a reliable and good correspondence between the theoretical prediction and the experimental measurements. In all measurements, we define a contour as the boundary of the avalanche which passes through those points of the chute which are approximately covered (in height) at least by a single grain of the granular material. Also note that the determination of such boundaries is relatively easy for experiments with the Big-Cap and with sand, but, it is difficult for Small-Cap experiments conducted with quartz particles.

10.2.9 Single Constituent Granulates

In the theory, we treat the granular mixture as a single constituent. In reality it is almost impossible to find geomaterials which consist of a single constituent. Sand, quartz or rice, whatever we use for a laboratory run, contain some dust, powder and small grains either because the material was not properly washed or abrasion occurs during the experiment. After several runs the situation becomes even worse. During the flow of an avalanche small particles move towards the bottom and the rear part of the avalanche, whereas the larger grains are carried to the surface and collected near the front of the avalanche. This is a consequence of kinetic sieving during the dynamics of the avalanche. Therefore, (at least) it is not so easy to control the friction angle between the avalanching material and the chute and between the grains themselves. This could make the bed friction angle position dependent. Nevertheless, in all experiments we tried to maintain the possible optimal choice by cleaning the chute after each experiment and filling the caps more homogeneously. Therefore, one should always remember, while comparing the experimental results with the theory, that such factors are also responsible for possible discrepancies.

10.3 Validation of the Theory

One of our major aims is the validation of the theory by some laboratory experiments. In this section we will present some selected results of non-steady and free-surface avalanche flow of granular materials in a laboratory chute against the theoretical prediction. Particularly, we will demonstrate how good is the theoretical prediction of velocity distribution of an unsteady flow avalanche down a curved chute against PIV-measurements of the velocity field of the particles at different parts of the free-surface.

10.3.1 Experiments Using Small-Cap and Quartz Particles[‡]

Figure 10.1 depicts a series of experimental snapshots of an avalanche in the laboratory. A bulk material of quartz granulates is held by the Small Cap. The first panel shows a photograph immediately before the lifting of the cap defining the initial condition of the avalanche, whereas the second panel describes the circumstances right after the opening of the cap. As soon as the cap is opened the bulk material extends in all directions, but mainly in the down-hill direction due to the gravitational acceleration. The body is continuously extending in the direction of steepest descent. Panel three captures the fully developed flow in which the entire part lies in the upper inclined zone. Comparing the first, second and third panels one can see that the front of the avalanche accelerates faster than its tail. The reason for this is that the entire heap is under a passive state of stress before the cap is lifted. Immediately after the release of the cap the front part of the heap no longer suffers a surface stress from the confining cap, and an active state of earth pressure is established. The remaining grains still feel the stresses from their neighbours (which is the passive stress) until the wave front that separates the active from the passive states has reached the upper part. So, the motion of the frontal part of the pile is ahead of that in the rear portion. Moreover, the initial surface slope triggers a downhill motion, whereas that in the rear part acts in the uphill direction. In panel four, the avalanche has entered the transition zone. The front of the avalanche has just crossed the front boundary of the transition zone and has entered the deposition zone. Due to the down-slope curvature of the chute topography in the transition zone the avalanching front starts decelerating. Therefore, the mass in the front is contracting in the downhill direction due to the effect of the passive earth pressure, but the mass in the tail is still extending. The deposition of the mass commences in the vicinity of the lower end of the transition zone. The fifth panel captures a snap of the avalanche at a time when the major part of the body lies in the run-out zone and the body is approaching its rest position. The rear material is now hindered from freely moving forward; it dilates now in the cross-slope direction and begins to broaden its deposition. The far end part of the tail consists mainly of the fine granulates and the powder is an inevitable constituent of the bulk material. The final panel shows the deposit of the avalanche which lies entirely in the horizontal run-out zone of the chute. Although (immediately before the deposit) the front of the body is almost at stand still the mass from the tail is continuously flowing down and is deposited on the tail side of the body. A steep surface (height) gradient is thus developed on the tail side of the avalanche. Occasionally, this steep backward slope is slightly weakened in the last phase of the motion by a backward motion of the top granules

[‡]These experiments were jointly conducted with Prof. S.-S. Hsiau, a A. v. Humboldt fellow from National Central University, Chung-Li, Taiwan.

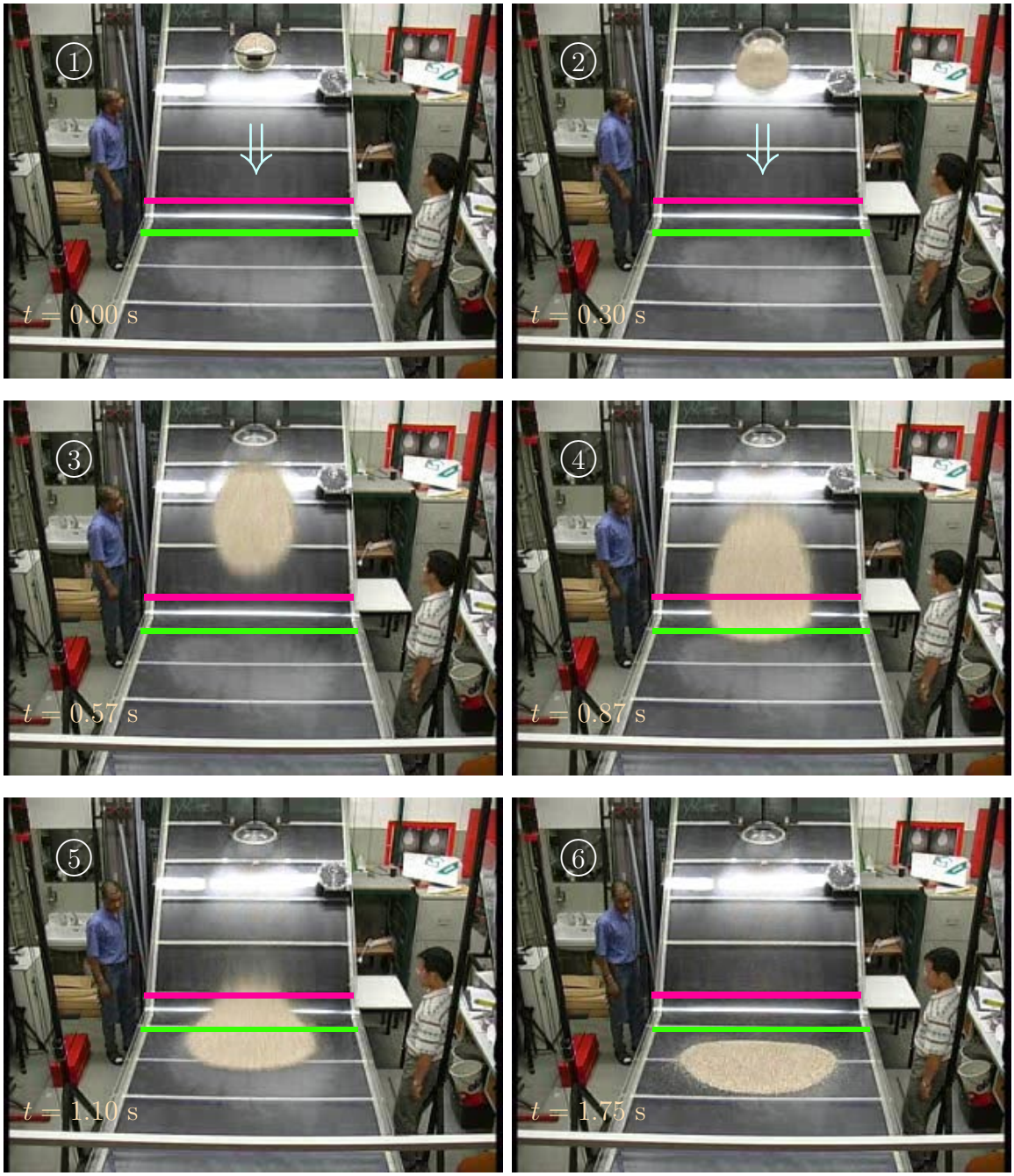

Figure 10.1: Overview of the laboratory avalanche chute with six snapshots of a sand avalanche, showing the spreading mass from initiation (first panel) to deposition (sixth panel), lasting approximately 1.75 seconds. The chute (4000 mm long and 1600 mm wide) is made of plexiglass. The upper plane part is inclined at 45°; it merges into a short cylindrical element with rear boundary at 1560 mm and front boundary at 1930 mm from the top of the chute. These boundaries are indicated by red and green lines, respectively. It is followed by the horizontal run-out plane. The sand is initially held in a hemi-spherical cap that is quickly upward tilted to release the material, which here is quartz of 4 mm nominal diameter. On the upper right edge of the chute an analog watch indicates the time. The arrows in the first two panels show the direction of the downhill motion, the circled numbers indicate the consecutive orders of the snapshots and the real times are shown on the lower left corners. Note the somewhat blurred margins of the piles due to collisions. The persons are: left: the author, right: Prof. S.-S. Hsiau

to reestablish the local angle of repose. The deposit is seen to be a good continuum of granulates. Its shape is convex, more or less ellipsoidal with major axis along the lateral direction. Actually, in all panels the flowing granular body is fairly compact with only slightly diffusive margins due to particle bouncing so that the continuum assumption seems to be justified. The shape of the body depends on the material properties, i.e., internal and bed friction angles, the chute geometry, the geometry of the material in its initial position and the initial conditions. The motion of the bulk and deforming body from panel one to panel six defines the complete dynamics of the avalanche as a rapid free-surface motion of dry granular material from initiation to deposit.

10.3.2 The PIV-Measurement and Validation of the Theory

One of the dynamical aspects of an avalanche is its velocity distribution. It is very important for practitioners to have proper knowledge of the velocity field in order to estimate the impact pressures (on obstructions and infrastructures), stress and strain rate, and so on along the track of a sliding avalanche down a mountain topography. From a structural engineering and planning point of view one must know the velocity field properly in order to adequately design buildings, roadways and rail transportations in mountainous regions and properly predict the impact pressures on obstructing buildings that may be hit by an avalanche. Equally important is to know the velocity field of flowing granular materials and fine granulates through various channels in process engineering scenarios to predict the flow dynamics. In this regard we present now some results concerning the velocity field obtained by using the PIV-measurements of an avalanche of quartz particles flowing down a curved chute, (see, Fig. 10.1) and compare it with the theoretical prediction. We will see in the sequel that there is rather good agreement between theory and measurements.

Before presenting a close and detailed comparison between theory and measurements, it should be mentioned that in some cases the lengths of the panels deduced from the experimental measurements do not exactly correspond to their theoretical counterparts. The reason for this is the relatively small (physical) domain, captured by the cameras. We have used the best possible set-up and equipments, but the room in the laboratory was fairly small and constrained our flexibilities. The cameras were able to capture images only in various subregions of the chute. In fact, the following figures show the full frames captured by the camera(s) (see panels on the right of Fig. 10.2). This implies that consecutive pictures correspond to different experiments, repetitions under identical external conditions. Finally, note that the different colours in these pictures represent the magnitudes of a kind of mean velocity distribution in the corresponding regions determined by the contours computed from the real data of the velocity magnitudes. The magnitudes of the velocity fields are shown in the right colourbars of each picture. It should therefore be clear that the real range of the actual velocity field may be somewhat larger than that presented here. Since we have plotted the mean velocity for both the measurements and theoretical predictions, there is no question of inconsistency. As we increase the number of contours, the range of the colourbars may equally increase. Also, the arrows indicate the directions, and their lengths represent the relative magnitudes of the actual velocity vectors. One further remark is that we wanted to have good images of the laboratory runs in all zones, the upper inclined zone, the middle transition-zone and the run-out zone.

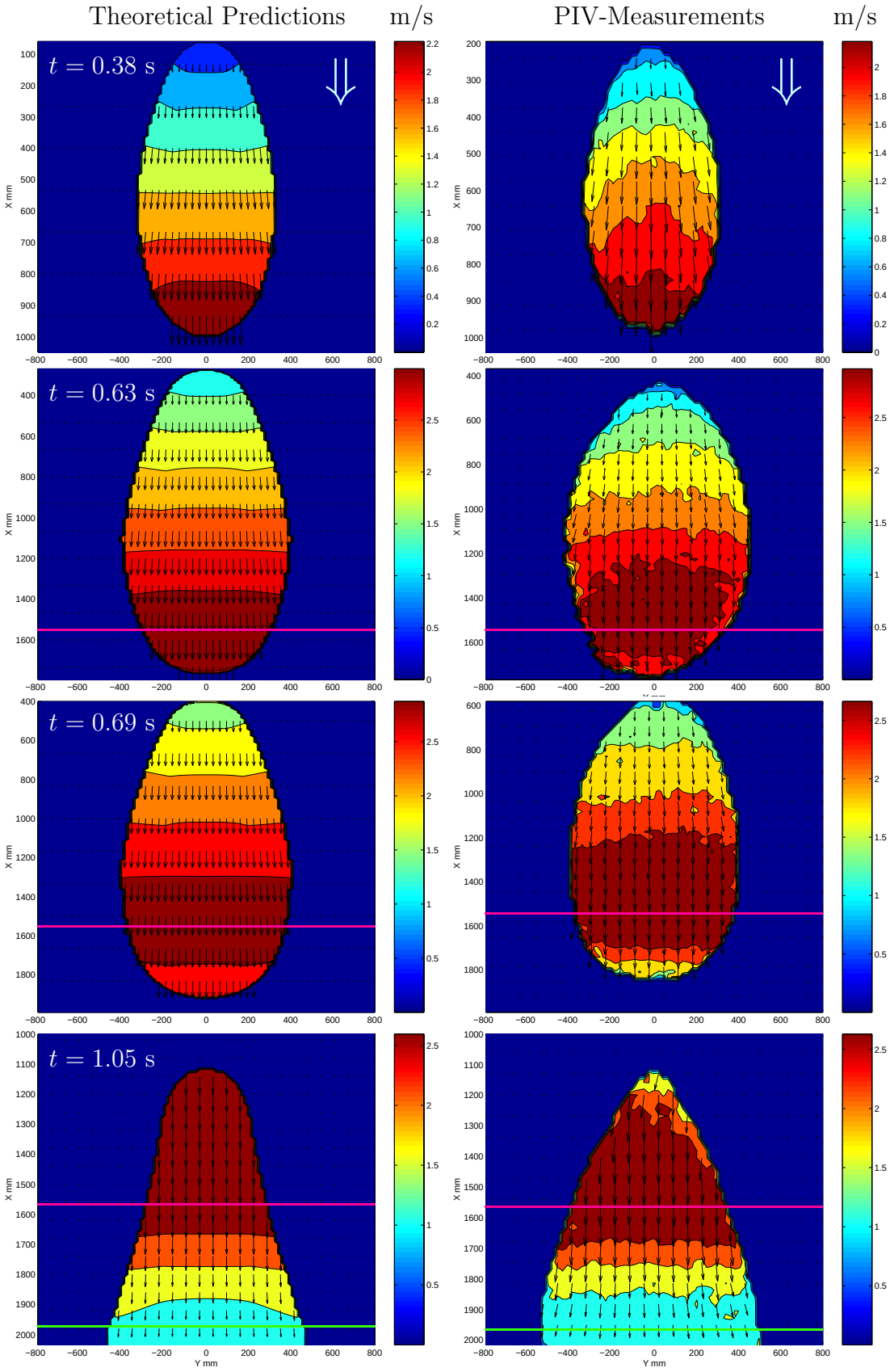

Figure 10.2: Comparison between pile geometries and the velocity distributions at the surface according to the theoretical prediction (left panels) and the PIV-measurements (right panels). The experimental configuration is explained and presented in Fig. 10.1. Direct comparison demonstrates excellent agreement between theory and experimental measurements of the geometry and the velocity distribution as the avalanche slides down an inclined surface merging into the horizontal run-out zone

In general it is a very difficult task to have an appropriate image in a region one wishes to capture. This is due to the low temporal resolution of the CCD-cameras (note that they allow only about 4 double frames for one camera and only about 2 double frames for two cameras per second), the relatively large chute, the restricted availability of space and the restricted capabilities of the lenses. The reason for using a relatively large chute is to acquire a better understanding of the physics of the fully developed unsteady flow dynamics in all regions of the whole flow domain. Nevertheless, the results presented here are for the best snapshots in each region of the chute, and this required to perform several experiments for one set of external conditions.

Figure 10.2 depicts a comparison between the theoretical predictions (left panels) and the PIV-measurements (right panels) of an avalanche of a bulk material composed of quartz particles sliding and deforming down a curved plexiglass chute as shown and explained in Fig. 10.1. The comparison is presented at four consecutive times as indicated in the upper left corners of each panel immediately after the onset of the motion of an avalanche until it crosses the horizontal run-out zone.

The two upper most panels of Fig. 10.2 present the theoretical versus the experimental results at time 0.38 s. The flow is fully developed, unsteady and the granular mass lies entirely on the inclined upper-zone of the chute. The motion is mainly in the down-hill direction (with some sidewise spreading), accelerating, and the velocity field is symmetric about the central line ($y = 0$) of the chute. The colourbars to the right of each picture indicate the magnitudes of the velocity fields in ms^{-1}. Differences are only seen in the curvature of the lines separating the differently coloured velocity regions. Apart from this, comparison of the two panels shows an excellent agreement between theory and experiment for both the geometry (boundary) and the velocity distribution of the avalanche of quartz particles for this time step. Note that this agreement could even be improved if the unfiltered velocity data would be smoothed.

The second row contains the theoretical and experimental results at time 0.63 s. A trace of a boundary layer effect along the margins can be seen in the experimental panel. As soon as the mass crosses the upper boundary of the transition zone (horizontal red line) the flow switches to the subcritical state from its supercritical state, and the mass starts decelerating. This is seen in both panels, but most clearly in the experimental one, in which the velocity reduction at the front tip of the margin seems to be somewhat larger. Otherwise, the measured pile is a bit wider than the computed one, and in the rear the computed pile is rounder than the measured pile. The slight asymmetry of the measured pile cannot be explained. This asymmetry seems to disappear as the pile moves on. Apart from this, there is very good correspondence between the prediction of the theory and the PIV-measurement.

At time 0.69 s (panels of row three) a large portion of the mass has been entered into the transition zone. At this time the transition of the flow from a supercritical to a subcritical state can be clearly seen in both panels. As explained before, this is the effect of the curvature of the chute in the down-hill direction. Although the body is contracting around its front, it is still extending in its rear part. Comparing the experimental and computed velocity distributions and the pile geometries, it is seen that the symmetry of the experimental avalanche pile is not yet fully established. In addition, the computed

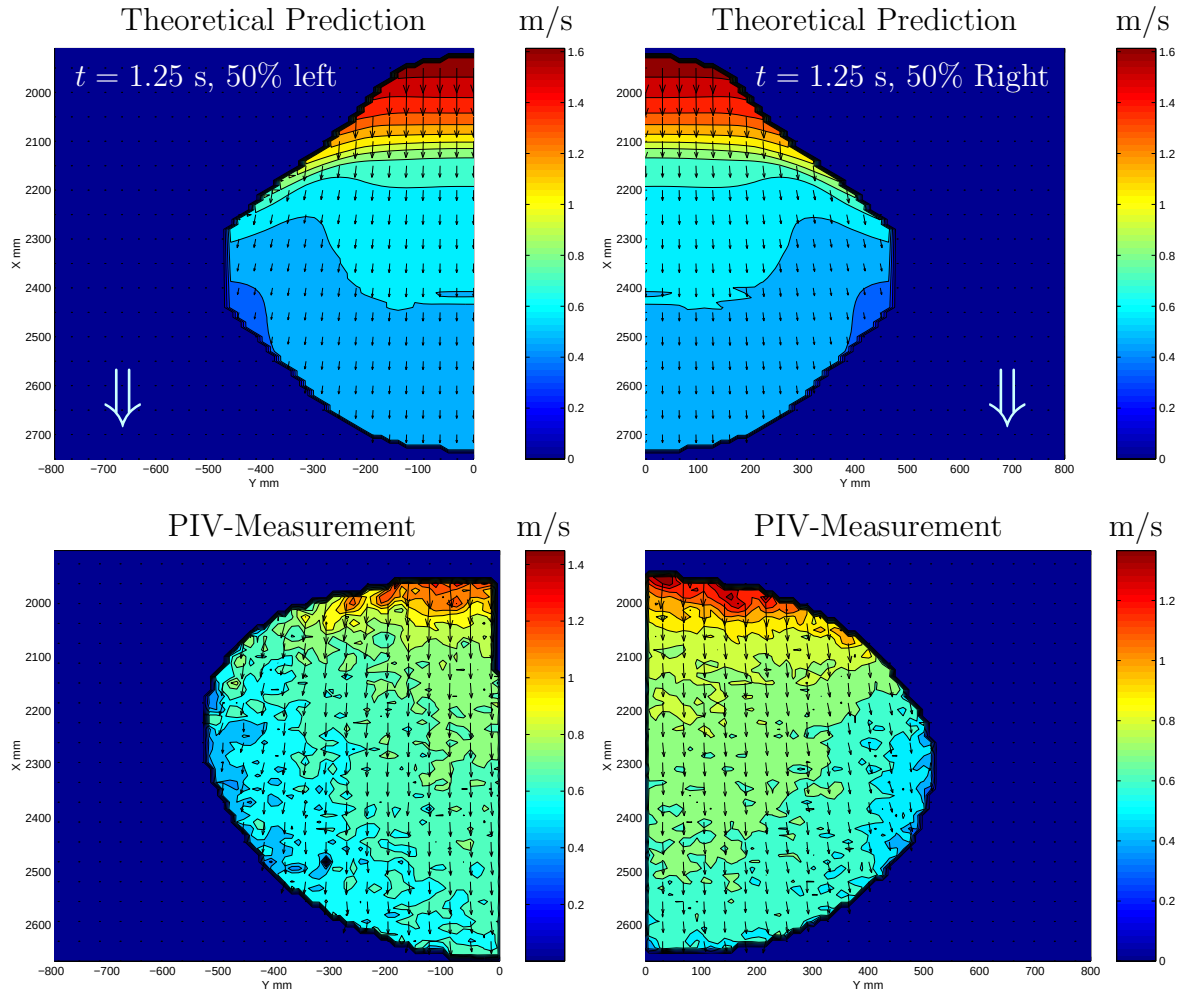

Figure 10.3: Avalanche near its deposit in the horizontal run-out zone at time 1.25 s. The entire body of avalanche is divided into two equal parts left and right in both the theoretical (upper panels) and the experimental measurements (lower panels). Experimental panels are captured by two CCD-cameras

pile is longer and its front and rear ends more advanced and more retracted than in the experiment. So, the coincidence of the two is fair.

A special situation is presented in the final row (time 1.05 s) in the sense that these panels only show the rear part of the pile (only this part was covered by the camera). Furthermore, the panels include the motion of the avalanche in all three parts: the upper inclined zone, middle transition zone and the lower run-out zone. A close look at the lower parts of both panels reveals that the granular body is contracting around its front in the run-out zone. Since the chute is laterally unconfined the granular mass is extending in the cross-slope direction near the front. This spreading is symmetric about the central line. The longitudinal earth pressure is increasing (passive pressure state), and this information is propagating upstream. This can clearly be observed if we compare these panels with the panels of the third row, because the magnitude of the velocity field has considerably decreased. On the other hand, the cross-slope earth pressure is decreasing (active pressure state). This information is also propagating upstream. As soon as the

mass enters the run-out zone the velocities of the particles decrease rapidly. Consequently, the mass is extending in the lateral direction. The extent of the granular pile and the velocity distributions compare in these panels rather well. However, the rear margin is far more pointed in the experimental pile than in its computed counterpart. The reasons for this behaviour are not known at present and call for further scrutiny. Comparison of the theoretical prediction with the experimental result reveal an excellent agreement.

Figure 10.3 describes the state of the avalanching mass just before it comes to rest at the time 1.25 s. The entire mass of the body now lies in the horizontal run-out zone. The total mass is now divided into two equal parts both for the theoretical computations (upper-panels) and its experimental counterparts (lower panels). The left and right panels (in both theoretical and experimental cases) are almost symmetrical about the central line ($y = 0$) of the chute. Although the particles around the rear ends are still considerably in motion, those near the front of the body are close to their rest position. Note that, although the colour distribution does not seem to correspond to each other between theory and measurement, their numerical values agree quite well. The discrepancy in the shape of the pile body is also due to the contour plotting because it neglects that part of the body which has very small velocity magnitude. Apart from this, the lateral and longitudinal spread of the body and velocity distributions are both in a very good agreement between the theoretical predictions and the experimental measurements.

10.3.3 Evolution of the Avalanche Geometry

We have seen in the last subsection that the PIV-measurements can obviously be used to determine the avalanche boundary. Since the applied technique is only apt for the velocity measurements we can not use it to determine the three-dimensional evolution of the avalanche geometry. For this we need to apply some other techniques like digital photogrammetry. One of the most important aspects in avalanche dynamics is the determination of the run-out area and the height profile of the avalanche in its deposit. This is so, because with this information we can construct the hazard map and estimate the impact pressures on the obstructions in the run-out zone. The evolution of the three-dimensional geometry along the entire track is not so vital. For this reason we measured the avalanche height in the deposit using a penetrometer. Figure 10.4 displays the flood-contours of the depths of the avalanche in the deposition area both for the theoretical prediction and the experimental measurement at times ≥ 1.35 s as the avalanche comes to rest. Note that the deep blue contour (patch) of the experimental panel has almost zero value. Disregarding this patch it is clearly seen that the lateral and the longitudinal run-out distances, the over all run-out zone as well as the height profiles are well predicted by the theory.

10.3.4 Velocity Measurements from the Top and Bottom

The avalanche equations, developed by us to predict the velocity and evolution of the avalanche geometry, are based on realistic assumptions. One of them concerns the velocity distribution through the depth. We have assumed that the velocity profile is almost uniform through the depth of the avalanche. This assumption may not be a good one right after the release, around the obstructions and close to the deposit where both the

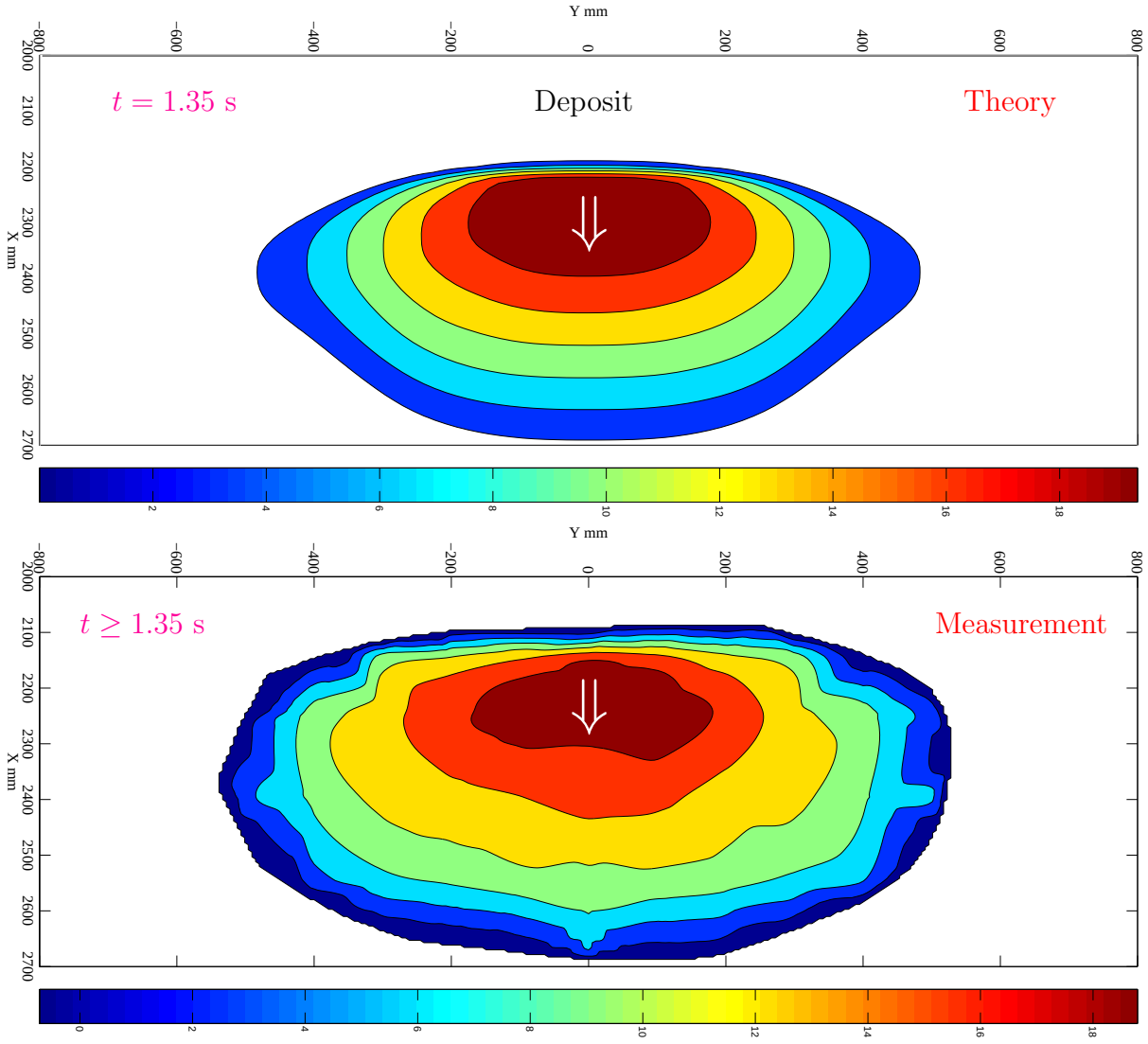

Figure 10.4: Final deposit of the avalanche: The contours in the upper panel represent the computed avalanche heights whereas the contours in the lower panel represent the measured heights, both in the horizontal run-out zone. The experimental result is well predicted by the theory

height and vertical component of the velocity field could change considerably; in some cases even abruptly. However, along the main flow path or the track of the avalanche, the concept of uniform velocity distribution through its depth should be a fairly reasonable assumption. This is not difficult to check whether it was only a "philosophical fantasy" or could describe the underlying physics of the flowing avalanche quite well. We performed several experiments for different granular materials and analysed the images just before the transition zone (so as to have both a fully developed unsteady flow and good quality and resolution of the images). Two cameras were placed and aligned parallel to the normal of the chute surface about 1000 mm distant from the chute on either side. Since we were using a plexiglass chute capturing images from either side of the chute was possible. The measured velocity distributions from top and bottom of the chute show that the differences between the mean velocities were less that 3% in all cases, providing the physical justification of our assumption.

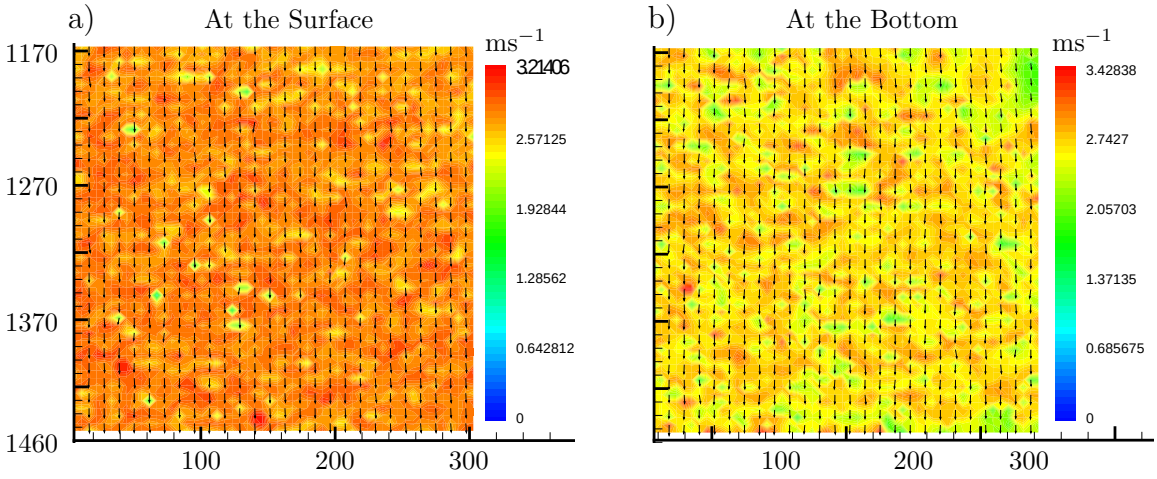

Figure 10.5: Velocity distribution over depth: a) at the free-surface, b) at the bottom. The actual topographic location of the chute is shown in length units in mm. The left velocity field is computed from the image captured by the camera from the top (free-surface) and the right field is its counterpart computed from the image captured simultaneously by another camera from the opposite side (bottom) of the plexiglass chute. To have a better visualisation the right field is mirrored about the central line of the chute

Figure 10.5a displays the velocity measurement at the free-surface of a fully developed avalanche of quartz particles initially kept in the small cap. The mean and the standard deviation are 2.75 ms^{-1} and 0.16, respectively. Similarly, Fig. 10.5b depicts the velocity field at the bottom of the avalanche measured from the opposite side of the plexiglass chute. To have better visualisation this field is mirrored about the central line ($y = 0$) of the chute. The mean and the standard deviation for this case are 2.67 ms^{-1} and 0.26, respectively. This indicates the fact that, although the absolute maximum value of the velocity field in the right figure is a bit higher than the left one, the mean velocity at the free-surface is slightly higher than the mean velocity at the bottom. The mean deviation is about 2.9%. The non-realistic higher absolute values in the right figure emerge from the measurement errors. There are two main error sources: First, being plexiglass, the chute is a bit scratched. These scratches produce random reflections. Second, reflections are also due to the horizontal metal bars (the supports of the chute). These reflections artificially increase the magnitude of the velocity field, but one can not say exactly how much. However, there is no problem of this kind for the image taken from the top of the chute because the plexiglass bed-surface is on the opposite side of this camera. The higher value of the standard deviation (for the right figure) also manifests the random fluctuation of the velocity field due to these reflections. Otherwise, the comparison between these two figures reveals the fact that for the fully developed motion of an avalanche the velocity distribution through the depth is fairly uniform.

Chapter 11

Summary and Outlook

There remain now two questions: What has been done so far and what should be done in future? The answer to the first question is relatively easy but very important to be realised in order to have an over all idea about the up-to-date achievements as well as the specific, significant and novel and lofty outcomes of the present research works. The straightforward answer to the second question seems to be a bit difficult but from the past experience, today's need and technology we can infer what can be and what must be done in future, first to provide continuity to the work we have done until now and utilise the achievements we have so far obtained in the real applications directly related to the security and benefits of the public. For the continuation of the research activities and the implementation of the results thus obtained, it is required in practice to use the most advanced technology both to understand the physics of the flow by means of some well controllable laboratory and field experiments and to corroborate the available, most advanced and sophisticated theoretical tool in different configurations that are compatible with the need of the people and are close to reality. Such tasks may be related to geophysical flows of large scale and catastrophic deformations and movements of earth materials like landslides, rockslides, debris and snow avalanches down the slopes of mountains. Understanding the mechanisms of the initiation and dynamics of the flows from the breaking of the masses to the depositions is extremely important for the hazard mappings of the mountain regions, for the prevention, reduction and mitigation of the natural hazards causing the devastating damage of properties and claiming the lives of the people to a large scale. Alternatively, one can make use of these theoretical and experimental facilities to analyse the flows of powders and fine granulates in silos, hoppers and the transportation of different kinds of bulk materials like cereals, ceramics, dyestuffs, electronic materials, pills and capsules, just to name a few, through different and specific channels in the food producing, chemical process and pharmaceutical industries. Prediction of such flows basically helps in the production and quality control of these materials to meet the standards set by the concerned authority.

To Present

Now, we go back to the first question. We were mainly involved in doing three things successively:

- development of a new and general theory for avalanching debris flows that can be of use both in geophysics and process engineering,

- implementation of reliable and sophisticated numerical methods that can appropriately solve the model equations thus developed without loosing the underlying physics of the theory,

- and, finally, providing the proof that the theoretical predictions of the model equations can well be reproduced by the laboratory experiments so as to pave ways to real applications in different scenarios.

Theory: Concerning the theory we would like to emphasise the following points: The new model equations (4.85)–(4.87), developed in Chapter 4, are formally analogous to those of previous derivations under much simpler situations. For torsion-free and flat cross-slope (reference) bed topography these equations reduce to the much simpler equations proposed by GRAY et al. and WIELAND et al. [31, 131] as special cases. Furthermore, the new theory can reproduce all previous model equations of the Savage-Hutter theory as particular cases. Analysis of the motion of avalanches in channels with different cross-slope curvatures and widths is now possible. For the first time we were able to include the simultaneous effects of the curvature and torsion in the avalanche motion, which could not be achieved by previous models. This should be realised as one of the major advantages and achievements of these new model equations. The applicability of the present model equations is, therefore, much broader than in the previous cases. The advantage of this formulation of a depth–averaged avalanche model lies in its flexibility of application. The flow down an inclined plane or within a channel with its axis in a vertical plane which may be curved can be described, as can the flow down complicated mountain valleys with arbitrarily curved and twisted talwegs and bed topographies. It is this last application which has motivated us to derive the new model, because it is ideally suited to realistic situations in connection with the use of Geographical Information and Visualisation Systems (GIVS). Thus, the theory provides an entirely new direction in the field of avalanche and debris flow research. It also opens a large spectrum of applications in different industrial and geophysical problems. We simply mention at this point that *Modelling debris flow dynamics over non-trivial mountain topography and inclusion of bed erosion and deposition* are in progress [106].

Numerics: Another challenge has been to solve the model equations. The first step towards the full understanding of the theory is the simulation of the model equations for some specific and particularly interesting, somehow academic engineering problems. The results emerging from these simulations indicate the basic and fundamental capabilities of the entire theory. Since the model consists of non-linear hyperbolic partial differential equations with discontinuous coefficients we can not solve them with classical numerical methods. To avoid any spurious oscillations and include naturally induced shock phenomena of these hyperbolic equations we introduced shock-capturing numerical schemes. To this end, two-dimensional Non-Oscillatory Central (2D-NOC) schemes with Total Variation Diminishing (TVD)-limiters were implemented. The numerical sensitivity analysis reveals that the NOC method with Minmod limiter provides the best performance for the avalanche flows. One of the most interesting aspects of avalanche dynamics is the study of avalanching motion over different bed structures and the effect of topography on their motion and deposits. For this purpose a large number of simulations are presented for different topographic configurations. The first part of the simulations is concerned with a very simple bed topography that is laterally flat but curved and merges into the

horizontal run-out zone along the down-hill direction. One of the most basic and fundamental questions related to the new model equations is: are these model equations really able to predict flows in chutes and channels which simultaneously incorporate curvature and torsion effects of the bed topography? In other words, can we really use these equations to predict the flow dynamics of debris and avalanches down arbitrarily curved and twisted mountain valleys and natural gullies from initiation to deposit? To answer these questions, we performed several numerical tests for avalanching masses down curved and twisted bed topographies. Uniformly curved and twisted channels as well as channels which incorporate a continuous transition zone merging into the horizontal run-out zones are considered. Both, confined and unconfined transition zones with constant and variable inclination angle of the topography are taken into account. In one instance, the used topographies are based on helicoidal talwegs. As the "Arts" of the theory can be seen in the simulations, these computations reveal fantastic and fascinating results that we were imaging while developing the theory. They demonstrate the combined effects of curvature, torsion and the radial acceleration associated with the bed topography. Thus, we are able to quantify the intrinsic effects of the topography on the dynamics of flow avalanches. Such sophisticated studies have not been carried out before, and it was possible here only with the new model equations.

Experiments: A scientific work, whatever it may be, should be verified by observations on the natural object or some suitable experiments that are conducted in the laboratory. It should not merely be based on some computations, manipulations, reasonings and logics that are not physically verified. Practitioners and engineers will use or tend to use model equations which are already proven to be able to reproduce experimental facts either in the laboratory or in the field. Thus, in order to acquire confidence in new model equations it is vital to corroborate them by direct observation. In this spirit, we performed several laboratory experiments for different materials in order to check the validity of the theory. The two most important aspects of avalanche dynamics are probably: the velocity distribution and the evolution of the avalanche boundary from its initiation to the deposit in the run-out zone and the depth profile of the deposit. We used modern measurement technique, the Particle Image Velocimetry (PIV), to measure the velocity field of the particles at the free-surface and the bottom of the free-surface and unsteady motion of an unconfined avalanche over a chute that is curved in the main flow direction merging continuously into the horizontal run-out zone. Only selected results were presented here to show how the method works in reality. We presented the results for different regions of the chute and for different times. We were looking for the correspondence and harmony between the theory, the adequacy of the numerics and the demonstration of the experimental facts. We are able to demonstrate the fact that there are excellent agreements between the theoretical predictions of the model equations and the experimental measurements. This, ultimately, proves the applicability of the theory and efficiency of the numerical method and code and establishes a nice and strong correlation among the theory, numerics and the experiments. We have thus created a little science by means of modelling and predicted a tiny part of nature via experiments. In this way we were able to bring the science and nature together.

In Future

Now we address the second and final question we posed at the beginning: what should be done in future? Our experience says that there are still many challenges to be met

in the field of avalanche and debris flow research. Here we will focus only on the part of the problem related to dynamics. The main intention of research in this field should be directed towards modelling and solving the real problems so as to minimise the casualties and hazards induced by natural catastrophes like avalanches and debris disasters. This includes knowledge and understanding of the release mechanisms of avalanching masses, the reliable prediction of the motion from initiation to runout, the evaluation of impact forces of the moving masses on objects they may encounter, the estimation of the likelihood of an avalanche-prone region to be hit by a moving mass, etc. This list involves more than the scientific techniques provided in this thesis, but what has been attacked here is a vital subject of the overall theme. Within the limited scope, here is an outlook.

Application in Nature: Next and immediate goal should be to perform numerical simulations with the purpose of providing a general purpose software for practitioners involved in the prediction of avalanche run-out in mountainous regions. The intention should be the use of Geographical Information Systems (GIS) from which digitised realistic topographies in mountainous regions are available. With these GIS particular avalanche-prone subregions can be selected. From a preselected release of a finite mass of gravel or snow at a breaking zone the flow from initiation to run–out could then be determined. This step requires numerical integration via avalanche purpose-built software that incorporates a total–variation–diminishing non–oscillating scheme. Its output could, in a final step, be used in visualisation software to identify endangered zones. A multitude of applications could then be investigated with the software. Comparison with observational data in the field such as photographs from helicopters, or a digital video camera positioned at a fixed station, may then become possible. From these computational results one can easily estimate the impact pressures on obstructions and infrastructures along the track and in the deposit that is very useful for civil engineers, planers and authorities from municipalities who are responsible for the establishments in the mountain regions. Moreover, the results should ultimately be applied to construct hazard maps in the mountain ranges with the aim of avalanche warning, reduction, mitigation and prevention of (and from) the hazards.

Application in the Laboratory: Laboratory experiments can be used not only for the corroboration of the theoretical-numerical results, but equally as an alternative to test on a small scale the behaviour of an avalanching mass at a larger scale, as it occurs in nature. This method is particularly apt, because the SH-equations and their present extensions have been found to be scale independent. So, whenever the physical conditions are such that the SH-equations might be adequate, laboratory experiments might be advantageous to the computational approach. Furthermore, the effect of obstructions in an avalanche track can easily be studied by laboratory experiments. And with adequate pressure and shear gauges being used at walls of obstructions, such laboratory experiments may even be suitable to gain information about the forces exerted by avalanches on obstructing structures. Besides, laboratory experiments should be amply used to broaden the information on the corroboration of the theory.

Advancing the Numerics: Determination of the front and the entire boundary of the free-surface flow of avalanches is very important. From this one can probably more efficiently predict the front and boundary of the avalanche in time which may also be useful to increase the accuracy of the velocity distributions and the evolution of the avalanche geometry along its path and in the deposit. For this reason one needs to develop a

two-dimensional shock-capturing scheme that can be utilised for the moving boundary problem of the avalanche to determine the margin locations. For this, either one should incorporate the shock-capturing capability in the LAGRANGIAN moving grid scheme or one should develop new numerical methods in which the LAGRANGIAN method can somehow be inserted into the 2D-NOC schemes we have implemented here.

More Advanced Measurement Techniques and Experiments: As usual, the final step should be related to the experimental phenomena. There are lots of things to be done. From the technical side, one should increase the temporal resolution of the CCD-cameras so as to capture a larger number of experimental images during the flow of the avalanche. One may then obtain a better correspondence between theory and experiments. On the other hand, the PIV-measurement facility should be utilised to analyse avalanching flows over more complicated topographies. One can remodel the chute topography to include side-wise curvature, either uniform or non-uniform. The chute channel may either be diverging or converging in its main flow direction. Further complicated aspects would be to add more CCD-cameras and perform experiments for the flows over curved and twisted channels, as discussed above. The most interesting aspect would be the determination of the flow velocity by the PIV-measurement system for the flow of avalanches and debris sliding down a (more general) prototype mountain topography consisting of some realistic obstructions constructed, with the principle of down-scaling, in the laboratory environment, and then, use the measured results to predict the flow dynamics in the field. That would be a highly appreciable work.

Bibliography

[1] W. Ammann, O. Buser, U. Vollenwyder: *Lawinen* (Birkhäuser Verlag, Basel.Boston.Berlin, 1997)

[2] C. Ancey: 'Snow Avalanches'. In: *Geomorphological Fluid Mechanics*. Ed. by N. J. Balmforth, A. Provenzale (Springer, 2001) pp. 319–338

[3] C. Ancey, M. Meunier: Estimating bulk rheological properties of flowing avalanches from the field data. *Journal of Geophysical Research* (2003), submitted

[4] B. Armstrong, K. Williams: *The Avalanche Book* (Fulcrum, Golden, Colorado, 1986)

[5] H. Björnsson: 'Snow avalanche studies in Iceland'. In: *Avalanches. Glaciological Data Report GD-1* (World Data Center A for Glaciology, University of Colorado, Boulder, Co., 1977) pp. 39–42

[6] H. Björnsson: Avalanche activity in Iceland, climatic conditions, and terrain features. *J. Glaciol.* **26**(94), 13-23, (1980)

[7] J. Boussinesq: *Théorie Analytique de la Chaleur. Vol. 2* (Gathier-Villars, Paris, 1903)

[8] R. M. Bowen, C. –C. Wang: *Introduction to Vectors and Tensors: Volume 1–Linear and Multilinear Algebra* (Plenum Press, New York and London, 1976)

[9] R. M. Bowen, C. –C. Wang: *Introduction to Vectors and Tensors: Volume 2–Vector and Tensor Analysis* (Plenum Press, New York and London, 1976)

[10] L. Brillouin: *Tensors in mechanics and elasticity*, (Academic Press, New York, 1964)

[11] G. Brugnot: 'Recent progress and new applications of the dynamics of avalanches'. In: *Proc. Snow in Motion Symposium* (Intl. Glaciol. Soc., 1979)

[12] R. Courant, K. O. Friedrichs, H. Lewy: Uber die partiellen Differenzengleichungen der mathematisches Physik. *Math. Ann.* **100**, 32-74, (1928)

[13] R. Courant, K. O. Friedrichs, H. Lewy: On the partial differential equations of mathematical physics. *IBM Journal* **11**, 215-234, (1967)

[14] W. R. Dean: Note on the motion of fluid in a curved pipe. *Phil. Mag.* **4**(7), 208, (1927)

[15] W. R. Dean: The stream–line motion of fluid in a curved pipe. *Phil. Mag.* **5**(7), 673, (1928)

[16] R. P. Denlinger, R. M. Iverson: Flow of variably fluidised granular masses across three-dimensional terrain. 2. Numerical predictions and experimental tests. *J. Geophysical Research* **106**, 552-566, (2001)

[17] R. P. Denlinger, R. M. Iverson: Granular Avalanches Across Irregular Three-Dimensional Terrain: 1. Theory and Computation *J. Geophysical Research*, submitted, (2003)

[18] J. D. Dent, T. E. Lang: Modelling of snow flow. *J. Glaciology* **26**(94), 131-140, (1980)

[19] J. D. Dent, T. E. Lang: *Experiments on the mechanics of flowing snow.* Cold Reg. Sci. Tech., (1981)

[20] J. D. Dent, K. J. Burrel, D. S. Schmidt, M. Y. Louge, E. E. Adams, T. G. Jazbutis: Density, velocity and friction measurements in a dry–snow avalanche. *Annal. Glac.* **26**, 247-252, (1998)

[21] W. Eckart, J. M. N. T. Gray, K. Hutter: 'Particle Image Velocimetry (PIV) for Granular Avalanches on Inclined Planes'. In: *Lecture Notes in Applied and Computational Mechanics-LNACM Vol 11: Dynamic Response of Granular and Porous Materials under Large and Catastrophic Deformations.* Ed. by K. Hutter, N. Kirchner (Springer Verlag, 2003) pp. 195-218

[22] T. Erismann: Flowing, Rolling, Bouncing, Sliding: Synopsis of basic mechanisms. *Acta Mech.* **64**, 101-110, (1986)

[23] T. Erismann, G. Abele: *Dynamics of Rockslides and Rockfalls* (Springer Verlag, 2001)

[24] C. Fraser: *The Avalanches Enigma* (John Murray Publishers Ltd., Great Britain, 1966)

[25] C. Fraser: *Avalanches and Snow Safety* (John Murray Publishers Ltd., Great Britain, 1978)

[26] D. Gammack, P. E. Hydon: Flow in pipes with non-uniform curvature and torsion. *J. Fluid Mech.* **433**, 357-382, (2001)

[27] M. Germano: On the effect of torsion on helical pipe flow. *J. Fluid Mech.* **125**, 1-8, (1982)

[28] M. Germano: The Dean equations extended to a helical pipe flow. *J. Fluid Mech.* **203**, 289-305, (1989)

[29] J. M. N. T. Gray, K. Hutter: Pattern formation in granular avalanches. *Continuum Mech. Thermodyn.* **9**, 341-345, (1997)

[30] J. M. N. T. Gray, K. Hutter: Physik granularer Lawinen. *Physikalische Blätter* **54**, 37-43, (1998)

[31] J. M. N. T. Gray, M. Wieland, K. Hutter: Gravity-driven free surface flow of granular avalanches over complex basal topography. *Proc. R. Soc. London* A**455**, 1841-1874, (1999)

[32] J. M. N. T. Gray: Granular flow in partially filled slowly rotating drums. *J. Fluid Mech.* **441**, 1-29, (2001)

[33] J. M. N. T. Gray, Y.-C. Tai, S. Noelle: Shock waves, dead zones and particle free regions in rapid granular free surface flows. *J. Fluid Mech.* **491**, 160-181, (2003)

[34] R. Greve, K. Hutter: Motion of a granular avalanche in a convex and concave curved chute: experiments and theoretical predictions. *Phil. Trans. R. Soc. London* A**342**, 573-600, (1993)

[35] R. Greve, T. Koch, K. Hutter: Unconfined flow of granular avalanches along a partly curved surface. I. Theory. *Proc. R. Soc. London* A**445**, 399-413, (1994)

[36] H. -U. Gubler: 'Measurements and modelling of snow avalanche speeds'. In: *Avalanche Formation, Movement and Effects IAHS Publ. 162, September 14–19, 1986.* Ed. by B. Salm, H. -U. Gubler (IAHS, 1987) pp. 405–420

[37] P. K. Haff: Grain flow as a fluid-mechanical phenomenon. *J. Fluid Mech.* **134**, 401-430, (1983)

[38] A. Harten: High resolution schemes for hyperbolic conservation laws. *J. Comput. Phys.* **49**, 357–393, (1983)

[39] A. Harten, S. Osher, B. Engquist, R. Chakravarthy: Some results on uniformly high-order accurate essentially nonoscillatory schemes. *Applied Numerical Mathematics* **2**, 347–377, (1986)

[40] A. Heim: Bergsturz und Menschenleben. *Beiblatt zur Vierteljahresschrift der Naft. Ges. Zürich* **20**, 1-218, (1932)

[41] H. J. Herrmann, S. Luding: Modeling Granular Media on the Computer. *Continuum Mech. Thermodyn.* **10**, 189-231. (1998)

[42] K. Hsü: On sturzstorms - catastrophic debris streams generated by rockfalls. *Geol. Soc. Am. Bull.* **86**, 129-140, (1975)

[43] Ju-Jiang Hung: Typhoon Herb, the New-Central-Cross-Island-Highway and Slopeland Failures in Central Taiwan. *Sino-Geotechnique* **57**, 25-30, (1996)

[44] K. Hutter, F. Szidarovszky, S. Yakowitz: Plane steady shear flow of a cohesionless granular material down an inclined plane: a model for flow avalanches, Part I. Theory. *Acta Mech.* **63**, 87-112, (1986a)

[45] K. Hutter, F. Szidarovszky, S. Yakowitz: Plane steady shear flow of a cohesionless granular material down an inclined plane: a model for flow avalanches, Part II. Numerical results. *Acta Mech.* **65**, 239-261, (1986b)

[46] K. Hutter, Y. Nohguchi: Similarity solution for a Vollemy model of snow avalanches with finite mass. *Acta Mech.* **82**, 99-127, (1990)

[47] K. Hutter, T. Koch: Motion of a granular avalanche in an exponentially curved chute: experiments and theoretical predictions. *Phil. Trans. R. Soc. London* A**334**, 93-138, (1991)

[48] K. Hutter, R. Greve: Two-dimensional similarity solutions for finite-mass granular avalanches with Coulomb-type and viscous-type frictional resistance. *J. Glaciol.* **39**(132), 357-372, (1993)

[49] K. Hutter, M. Siegel, S. B. Savage, Y. Nohguchi: Two-dimensional spreading of a granular avalanche down an inclined plane. I. Theory. *Acta Mech.* **100**, 37-68, (1993)

[50] K. Hutter, K. R. Rajagopal: On flows of granular materials. *Continuum Mech. Thermodyn.* **6**, 81-139, (1994)

[51] K. Hutter, T. Koch, C. Plüss, S. B. Savage: Dynamics of avalanches of granular materials from initiation to runout. Part II: Experiments. *Acta Mech.* **109**, 127-165, (1995)

[52] K. Hutter: 'Avalanche Dynamics'. In: *Hydrology of Disaster*. Ed. by V. P. Singh (Kluwer Academic Publisher, the Netherlands, 1996) pp. 317-394

[53] K. Hutter, S. P. Pudasaini: Sind Lawienen, Hangrutschungen, Bergstürze und Muren berechenbare Elemente alpiner Naturgefahren? *Thema Forschung* **9**(2/2003), (ISSN 1434-7768), J 57936 T, 34-43, (2003)

[54] H. Hwang, K. Hutter: A new kinetic model for rapid granular flow. *Continuum Mech. Thermodyn.* **7**, 357-384, (1995)

[55] R. M. Iverson: The Physics of Debris Flows. *Reviews of Geophysics* **35**, 245-296, (1997)

[56] R. M. Iverson, R. P. Denlinger: Flow of variably fluidised granular masses across three-dimensional terrain. 1. Coulomb mixture theory. *J. Geophysical Research* **106**, 537-552, (2001)

[57] R. M. Iverson, M. Logan, R. P. Denlinger: Granular Avalanches Across Irregular Three-Dimensional Terrain: 2. Experimental Tests. *J. Geophysical Research*, submitted, (2003)

[58] J. T. Jenkins, S. B. Savage: A theory for the rapid flow of identical, smooth, nearly elastic particles. *J. Fluid Mech.* **130**, 186-202, (1983)

[59] J. T. Jenkins, M. W. Richman: Grad's 13-moment system for a dense gas of inelastic spheres. *Arch. Rat. Mech. Anal.* **87**, 355-377, (1985)

[60] J. T. Jenkins: 'Hydraulic Theory for a Frictional Debris Flow on a Collisional Shear Layer'. In: *Continuum Mechanics and Applications in Geophysics and in the Environment*. Ed. by B. Straughan, R. Greve, H. Ehrentraut, Y. Wang (Springer, 2001) pp. 113-125

[61] J. T. Jenkins, L. La Ragione: Particle spin in anisotropic granular materials. *Int. J. Solids Struct.* **38**, 1063-1069, (2001)

[62] G. S. Jiang, E. Tadmor: Nonoscillatory central schemes for multidimensional hyperbolic conservation laws. *SIAM J. Sci. Comput.* **19**, 1892–1917, (1998)

[63] R. D. Keane, R. J. Adrian: Theory of cross-correlation analysis of PIV images. *Applied Scientific Research* **49**, 191-215, (1992)

[64] S. Keller, Y. Ito, K. Nishimura: Measurements of the vertical velocity distribution in ping pong ball avalanches. *Annal. Clac.* **26**, 259-264, (1998)

[65] P. E. Kent: The transport mechanism in catastrophic rockfalls. *J. Geol.* **74**, 79-83, (1965)

[66] E. Klingbeil: *Tensorrechung für engenieure* (Bibliograshisches Institut, Mannheim: Hochschultaschenbücher, 1966)

[67] T. Koch, R. Greve, K. Hutter: Unconfined flow of granular avalanches along a partly curved chute. II. Experiments and numerical computations. *Proc. R. Soc. London* A **445**, 415-435, (1994)

[68] K. Koschdon, M. Schäfer: 'A Lagrangian-Eulerian finite-volume method for simulating free surface flows of granular avalanches'. In: *Lecture Notes in Applied and Computational Mechanics LNACM* **11***: Dynamic Response of Granular and Porous Materials under Large and Catastrophic Deformation*. Ed. by K. Hutter, N. Kirchner (Springer, 2003) pp. 83-108

[69] D. Kröner: *Numerical schemes for conservation laws* (B. G. Teubner Stuttgart, 1997)

[70] W. T. Lambe, R. V. Whitman: *Soil Mechanics* (Wiley & Sons, 1979)

[71] T. E. Lang, J. D. Dent: Review of surface friction, surface resistance and flow of snow. *Rev. of Geophys. & Space Phys.* **20**(1), 21-37, (1982)

[72] R. M. Lang: *An Experimental and Analytical Study on Gravity-Driven Free Surface Flow of Cohesionless Granular Media.* Ph. D. Thesis, Darmstadt University of Technology, Darmstadt, Germany, (1992)

[73] P. Lax: Weak solutions of nonlinear hyperbolic equations and their numerical computation. *Comm. Pure Appl. Math.* **7**, 159-193, (1954)

[74] R. J. LeVeque: *Numerical methods for conservation laws* (Birkhäuser Verlag, Basel, Boston, New York, 1990)

[75] K. A. Lie, S. Noelle: An improved quadrature rule for the flux-computation in staggered central difference schemes in multidimensions. *J. Sci. Computing.* **18**, 69-80, (2003)

[76] K. Lied, S. Bakkehøi: Empirical calculations of snow-avalanche run-out distance based on topographic parameters. *J. Glaciol.* **26**, 165-177, (1980)

[77] K. Lied, R. Toppe: Calculation of maximum snow avalanche runout distance based on topographic parameters identified by digital terrain models. *Proc. IGS symposium on snow and glacier research relating to human living conditions. Annals of Glaciology* **13**, 164, (1989)

[78] C. K. K. Lun, S. B. Savage, D. J. Jeffrey, N. Chepurniy: Kinetic theories for granular flows: inelastic particles in couette flow and slightly inelastic particles in general flow field. *J. Fluid Mech.* **140**, 223-256, (1984)

[79] D. M. McClung: Avalanche fatalities in Himalayan mountaineering. *American Alpine Journal* **23**(55), 138-145, (1981)

[80] D. M. McClung, K. Lied: Statistical and geometrical definition of snow avalanche runout. *Cold Reg. Sci. Technol.* **13**, 107-119, (1987)

[81] J. McElwaine, K. Nishimura: Ping–pong ball avalanche experiments. *Annal. Glac.* **32**, 241-250, (2001)

[82] M. Mellor: *Avalanches. Monogr.* III A3d, CRREL, (1968)

[83] J. Melosh: The physics of very large landslides. *Acta Mech.* **64**, 89-99, (1986)

[84] C. Mercier: Sur une representation des surfaces toroidales: applications aux equilibres magnetohydrodynamiques. *Fusion Nuclearie* **3**, 89-98, (1963)

[85] H. Nessyahu, E. Tadmor: Non-oscillatory central differencing for hyperbolic conservation laws. *J. Comput. Phys.* **87**, 408–463, (1990)

[86] Y. Nohguchi, K. Hutter, S. B. Savage: Similarity solutions for granular avalanches of finite mass with variable bed friction. *Continuum Mech. Thermodyn.* **1**, 239-265, (1989)

[87] A. K. Patra, A. C. Bauer, C. C. Nichita, E. B. Pitman, M. F. Sheridan, M. Bursik, B. Rupp, A. Weber, A. Stinto, L. Namikawa, C. Renschler: Parallel Adaptive Numerical Simulation of Day Avalanches over Natural Terrain. *J. Volcanology and Geothermal Research*, appearing, (2003)

[88] I. P. Perla, T. T. Cheng, D. M. McClung: A two-parameter model of snow avalanche motion. *J. Glaciology* **26**(94), 197-207, (1980)

[89] L. Piegl, W. Tiller: *The NURBS Book* (2nd edition, Springer, 1997)

[90] E. B. Pitman, C. C. Nichita, A. K. Patra, A. C. Bauer, M. Bursik, A. Weber: A Model of Granular Flows over an Erodible Surface. *Discrete and Continuous Dynamical Systems-Series B*, submitted, (2003)

[91] K. Pohlhausen: Zur näherungsweisen Integration der Differentialgleichung der laminaren Grenzschicht. *ZAMM* **1**, 252-268, (1921)

[92] J. G. Potyondy: Skin friction between soils and construction materials. *Geotechnique* **11**, 339-353 (1961)

[93] O. Pouliquen: Scaling laws in granular flows down rough inclined planes. *Physics of Fluids* **11** (3), 542-548, (1999)

[94] O. Pouliquen, Y. Forterre: Friction law for dense granular flows: application to the motion of a mass down a rough inclined plane. *J. Fluid Mech.* **453**, 133-151, (2002)

[95] Product information. *Metz Mecablitz*, (2000)

[96] Product information. *Nikon Nikkor Objektive*, (2000)

[97] S. P. Pudasaini, J. Mohring: Mathematical Model and Experimental Validation of Free Surface Size Segregation for Polydisperse Granular Materials. *Granular Matter* **4**, 45-56, (2002)

[98] S. P. Pudasaini, K. Hutter, W. Eckart: 'Gravity-Driven Rapid Shear Flows of Dry Granular Masses in Topographies with Orthogonal and Non-Orthogonal Metrics'. In: *Lecture Notes in Applied and Computational Mechanics- LNACM Vol 11: Dynamic Response of Granular and Porous Materials under Large and Catastrophic Deformations*. Ed. by K. Hutter, N. Kirchner (Springer Verlag, 2003) pp. 43-82

[99] S. P. Pudasaini, W. Eckart, K. Hutter: Gravity-Driven Rapid Shear Flows of Dry Granular Masses in Helically Curved and Twisted Channels. *Math. Models Meth. Appl. Sci.* **13**(7), 1019-1052, (2003)

[100] S. P. Pudasaini, K. Hutter: 'Granular Avalanche Model in Arbitrarily Curved and Twisted Mountain Terrain: a Basis for the Extension to Debris Flow'. In: *Debris-Flow Hazards Mitigation: Mechanics, Prediction and Assessment, Volume 1*. Ed. by D. Rickenmann, C.-l. Chen (Millpress, 2003) pp. 491-502

[101] S. P. Pudasaini, K. Hutter: Rapid Shear Flows of Dry Granular Masses Down Curved and Twisted Channels. *J. Fluid Mech.* **495**, 193-208, (2003)

[102] S. P. Pudasaini, Y. Wang, K. Hutter: Dynamics of Avalanches Along General Mountain Slopes. *Annal. Glac.* **38**, in press, (2004)

[103] S. P. Pudasaini, Y. Wang, K. Hutter: Porous Effects in the Description of the Dynamics of Granular Avalanches. *IUTAM-Symposium on the mechanics of physicochemical and electromechanical interactions in porous media, 18-23 May 2003, Kerkrade, The Netherlands*, (2003)

[104] S. P. Pudasaini, K. Hutter: Rapid motion of free-surface avalanches over natural terrains and their simulations through curved and twiste channels. *Philosophical Transactions A, the Royal Society, London*, submitted, (2003)

[105] S. P. Pudasaini, K. Hutter: *Avalanche Dynamics: Dynamics of Rapid Flows of Dense Granular Avalanches*, in progress, (2003)

[106] S. P. Pudasaini, K. Hutter: *Modelling Debris Flow Dynamics Over Non-Trivial Mountain Topography*, in progress, (2003)

[107] M. de Quervain, R. Meister: '50 years of snow profiles on the Weissfluhjoch and relations to the surrounding avalanche activity (1936/37–1985/86)'. *In: Avalanche Formation, Movement and Effects IAHS Publ. 162, September 14–19, 1986*. Ed. by B. Salm, H. -U. Gubler (IAHS, 1987) pp. 161–181

[108] M. Raffel, C. Willert, J. Kompenhans: *Particle Image Velocimetry* (Springer, 1998)

[109] B. Salm: 'Contribution to avalanche dynamics'. *IAHS AISH Publ. 69.* (IAHS, 1966) pp. 199–214

[110] B. Salm, H. Gubler: Measurement and Analysis of dense flow of avalanches. *Annal. Glac.* **6**, 26-34, (1985)

[111] S. B. Savage: 'Flow of granular materials'. In: *Theoretical and Applied Mechanics*. Ed. by P. Germain, M. Piau, D. Caillerie (Elsevier, 1989) pp. 241–266

[112] S. B. Savage, K. Hutter: The motion of a finite mass of granular material down a rough incline. *J. Fluid Mech.* **199**, 177-215, (1989)

[113] S. B. Savage, K. Hutter: Dynamics of avalanches of granular materials from initiation to runout. Part I: Analysis. *Acta Mech.* **86**, 201-223, (1991)

[114] R. L. Shreve: Shermann landslide Alaska. *Science* **154**, 1639-1643, (1966)

[115] W. Siemes, L. Hellmer: Die Messung der Wirbelschichtviskositat mit der pneumatischen Rinne. *Chem. Eng. Sci.* **17**, 555, (1962)

[116] V. P. Singh: 'Disasters: Natural or Man-made'. In: *Hydrology of Disaster*. Ed. by V. P. Singh (Kluwer Academic Publisher, the Netherlands, 1996) pp. 1–18

[117] I. S. Sokolnikoff: *Tensor analysis theory and applications* (Wiley, New York, 1951)

[118] L. S. Solove'v, V. D. Shafranov: Plasma confinement in closed magnetic system. *Rev. Plasma Phys.* **5** (New York: Consultants Bureau, 1970)

[119] T. Sonar: *Mehrdimensionale ENO-Verfahren* (B. G. Teubner Stuttgart, 1997)

[120] P. K. Sweby: High resolution schemes using flux limiters for hyperbolic conservation laws. *SIAM J. Numer. Anal.* **21**, 995–1101, (1984)

[121] Y. C. Tai : *Dynamics of Granular Avalanches and Their Simulations with Shock-Capturing and Front-Tracking Numerical Schemes*. Ph. D. Thesis, Darmstadt University of Technology, Darmstadt, Germany, (2000)

[122] Y. C. Tai, S. Noelle, J. M. N. T. Gray, K. Hutter: Shock-capturing and front-tracking methods for granular avalanches. *J. Comput. Phys.* **175**, 269–301, (2002)

[123] J. Tejchman, W. Wu: Experimental and numerical study of sand-steal interfaces. *Int. J. Num. and Anal. Methods in Geomech.* **19**, 513–536, (1995)

[124] E. F. Toro: *Riemann solvers and numerical methods for fluid dynamics* (2nd edition Springer-Verlag, 1999)

[125] E. F. Toro: *Shock-Capturing Methods for Free-Surface Shallow Flows* (John Wiley & Sons Ltd, 2001)

[126] G. Tóth, D. Odstrčil: Comparison of some Flux Corrected Transport and Total Variation Diminishing Numerical Schemes for Hydrodynamic and Magnetohydrodynamic Priblems. *J. Comput. Phy.* **128**(1), 82-100, (1996)

[127] A. Voellmy: Über die Zerstörungskraft von Lawinen. *Schweizeriche Bauzeitung* **73**, 159-162, 212-217, 246-249, 280-285, (1955)

[128] Th. von Kármán: Über laminare und turbulente Reibung. *ZAMM* **1**, 233-252, (1921)

[129] Y. Wang, K. Hutter: Comparisons of numerical methods with respect to convectively-dominated problems. *Int. J. Numer. Methods in Fluids* **37**, 721–745, (2001)

[130] Y. Wang, K. Hutter, S. P. Pudasaini: The Savage-Hutter Theory: a System of Partial Differential Equations for Avalanche Flows of Snow, Debris and Mud. *ZAMM - Journal of Applied Mathematics and Mechanics*, in press, (2004)

[131] M. Wieland, J. M. N. T. Gray, K. Hutter : Channelized free-surface flow of cohessionless granular avalanches in a chute with shallow lateral curvature. *J. Fluid Mech.* **392**, 73-100, (1999)

[132] H. C. Yee: Construction of explicit and implicit symmetric TVD schemes and their applications. *J. Comput. Phys.* **68**, 151-179, (1987)

[133] L. Zabielski, A. J. Mestel: Steady flow in a helically symmetric pipe. *J. Fluid Mech.* **370**, 297-320, (1998)

[134] L. Zabielski, A. J. Mestel: Unsteady blood flow in a helically symmetric pipe. *J. Fluid Mech.* **370**, 321-345, (1998)

[135] T. Zwinger: *Dynamics of Dry Snow Avalanches on Natural Terrains.* Ph. D. Thesis, Vienna University of Technology, Austria, (2000)

[136] T. Zwinger, A. Kluwick, P. Sampl: 'Numerical Simulation of Dry-Snow Avalanche Flow over Natural Terrain'. In: *Lecture Notes in Applied and Computational Mechanics- LNACM Vol 11: Dynamic Response of Granular and Porous Materials under Large and Catastrophic Deformations.* Ed. by K. Hutter, N. Kirchner (Springer Verlag, 2003) pp. 161-194

[137] $http://www.spiegel.de/panorama/0,1518,98158,00.html$

[138] $http://www.rcsd.k12.ms.us/{\sim}web08/bhs\_main/teachers/WEB\_JHOLLIS/avalanches2.htm$

[139] $http://www.natives.co.uk/news/2001/1101/25ava.htm$

[140] $http://www.pbs.org/newshour/bb/weather/jan-june99/snow\_2-25.html$

[141] $http://www.crealp.ch/en/contenu/crealp\_gondo\_photos.asp$

[142] $http://www.solarviews.com/eng/mars.htm$

[143] $http://www.earthsci.unimelb.edu.au/mars/Avalanche.html$

[144] $http://www.nepalnews.com/$

[145] $http://www.emergency.com/turkydis.htm$

[146] $http://vulcan.wr.usgs.gov/Volcanoes/MSH/May18/summary\_may18\_eruption.html$

[147] $http://www.tsi.com/$

Curriculum Vitae

Personal Data

Name:	Shiva Prasad Pudasaini
Address:	Pruthstrasse 10, 64295, Darmstadt, Germany
Date and place of birth:	21.10.1964, Bhadrawas, Kathmandu, Nepal
Marital status:	Married since 20.06.1995, three children

Schools and Universities

Ph. D. student since 26 September 2000:	Department of Mechanics Darmstadt University of Technology, Germany
M. Sc. nat., 2000:	Department of Mathematics University of Kaiserslautern, Germany (in Industrial Mathematics)
Master's degree, 1994:	Central Department of Mathematics Tribhuvan University, Kathmandu, Nepal (in Mathematics)
Bachelor's degree, 1991:	R. R. Campus Tribhuvan University, Kathmandu, Nepal (in Mathematics and Economics)
Secondary school, 1983:	Shree Adarsha Higher Secondary School Bhadrawas, Kathmandu, Nepal
Primary school, 1977:	Shree Saraswati Secondary School Thakalmath, Bhaktapur, Nepal

Professional experience

DFG-Hu 414/33-1 Grant 01/2003-12/2003	For research in Avalanche Dynamics in Complex Topography, Darmstadt University of Technology, Germany
SFB-298 Grant 09/2000-12/2002:	For research in Avalanche Dynamics, Darmstadt University of Technology, Germany
DAAD Scholarship 08/1998-09/2000:	For Master's degree in Industrial Mathematics University of Kaiserslautern, Germany
Assistant Lecturer 02/1996-04/1998:	Central Department of Mathematics Tribhuvan University, Kathmandu, Nepal
Junior Professor 09/1996-12/1996:	Nepal Engineering College Lalitpur, Nepal